

# mRNA reading frame maintenance during eukaryotic ribosome translocation

<https://doi.org/10.1038/s41586-023-06780-4>

Received: 21 April 2023

Accepted: 24 October 2023

Published online: 29 November 2023

 Check for updates

Nemanja Milicevic<sup>1</sup>, Lasse Jenner<sup>1</sup>, Alexander Myasnikov<sup>2</sup>, Marat Yusupov<sup>1</sup> & Gulnara Yusupova<sup>1</sup>✉

One of the most critical steps of protein synthesis is coupled translocation of messenger RNA (mRNA) and transfer RNAs (tRNAs) required to advance the mRNA reading frame by one codon. In eukaryotes, translocation is accelerated and its fidelity is maintained by elongation factor 2 (eEF2)<sup>1,2</sup>. At present, only a few snapshots of eukaryotic ribosome translocation have been reported<sup>3–5</sup>. Here we report ten high-resolution cryogenic-electron microscopy (cryo-EM) structures of the elongating eukaryotic ribosome bound to the full translocation module consisting of mRNA, peptidyl-tRNA and deacylated tRNA, seven of which also contained ribosome-bound, naturally modified eEF2. This study recapitulates mRNA-tRNA<sub>2</sub>-growing peptide module progression through the ribosome, from the earliest states of eEF2 translocase accommodation until the very late stages of the process, and shows an intricate network of interactions preventing the slippage of the translational reading frame. We demonstrate how the accuracy of eukaryotic translocation relies on eukaryote-specific elements of the 80S ribosome, eEF2 and tRNAs. Our findings shed light on the mechanism of translation arrest by the anti-fungal eEF2-binding inhibitor, sordarin. We also propose that the sterically constrained environment imposed by diphthamide, a conserved eukaryotic posttranslational modification in eEF2, not only stabilizes correct Watson–Crick codon–anticodon interactions but may also uncover erroneous peptidyl-tRNA, and therefore contribute to higher accuracy of protein synthesis in eukaryotes.

During protein synthesis, mRNA and tRNA must be rapidly translocated through the ribosome to advance the translational reading frame by one codon. The process is susceptible to errors, of which the most severe is shifting of the translational reading frame of mRNA, causing incorrect reading of succeeding codons. The key question is how does the eukaryotic ribosome couple mRNA and tRNA translocation during protein synthesis while securing the integrity of weak codon–anticodon interactions and thus preventing frameshifting? Many bacterial ribosome intermediates of translocation have been structurally analysed using both X-ray crystallography and cryo-EM<sup>6–11</sup>, however, insights into eukaryotic translocation complexes have been hindered by low-to-intermediate resolution<sup>3–5</sup>. The higher complexity of the eukaryotic 80S ribosome, with roughly 40% higher molecular mass than its prokaryotic counterpart and a minimum mass of 3.3 MDa in yeast and plants, hampered the high-resolution structural study of eukaryotic translocation, arguably the most complex operation of protein synthesis. Apart from being more sophisticated in terms of function and regulation<sup>12–14</sup>, an increasing number of genetic and biochemical studies report that the eukaryotic translational apparatus relies to a large extent on unique posttranscriptional modifications of ribosomal RNA (rRNA) and tRNAs, as well as kingdom-specific elongation factors, which actively contribute to the accuracy of protein synthesis.

In eukaryotes, the process of translocation is ensured by a five-domain GTPase, eEF2. Eukaryotic eEF2 and archaeal aEF2, contain a unique and strictly conserved posttranslationally modified histidine residue located at the tip of domain IV, named diphthamide, and shown to contribute to translation accuracy<sup>1,2</sup>. Its biosynthesis pathway requires the action of at least seven enzymes and even involves non-canonical radical enzyme chemistry. Diphthamide in human eEF2 is a target of at least two virulent toxins that inactivate eEF2 by ADP-ribosylation and cause lethal effects<sup>1,15,16</sup>. By failing to respond to high oxidative stress, mammalian cells lacking diphthamide are more sensitive to cell death<sup>17</sup>. Moreover, the loss of diphthamide can lead to several neurodegenerative diseases<sup>18,19</sup> and render human cells hypersensitive to tumour necrosis factor-mediated apoptosis<sup>20</sup>. A recent crystal structure of the *Saccharomyces cerevisiae* ribosome translocation intermediate (TI) revealed that domain IV of eEF2 and diphthamide engaged in an extensive stabilization network with the codon–anticodon duplex in an early state of translocation<sup>3</sup>, however, the role of diphthamide in other translocation phases remained unanswered.

We determined ten high-resolution cryo-EM structures (up to 1.97 Å) of elongating eukaryotic *S. cerevisiae* ribosome bound to the full translocation module consisting of mRNA, peptidyl-tRNA and deacylated tRNA, seven of which also contained ribosome-bound *S. cerevisiae* eEF2. Such a collection of TIs trapped in transition from the early to the late

<sup>1</sup>Institute of Genetics and Molecular and Cellular Biology (IGBMC), CNRS UMR7104, INSERM U1258, University of Strasbourg, Strasbourg, France. <sup>2</sup>Dubochet Center for Imaging (DCI), EPFL, Lausanne, Switzerland. ✉e-mail: gula@igbmc.fr

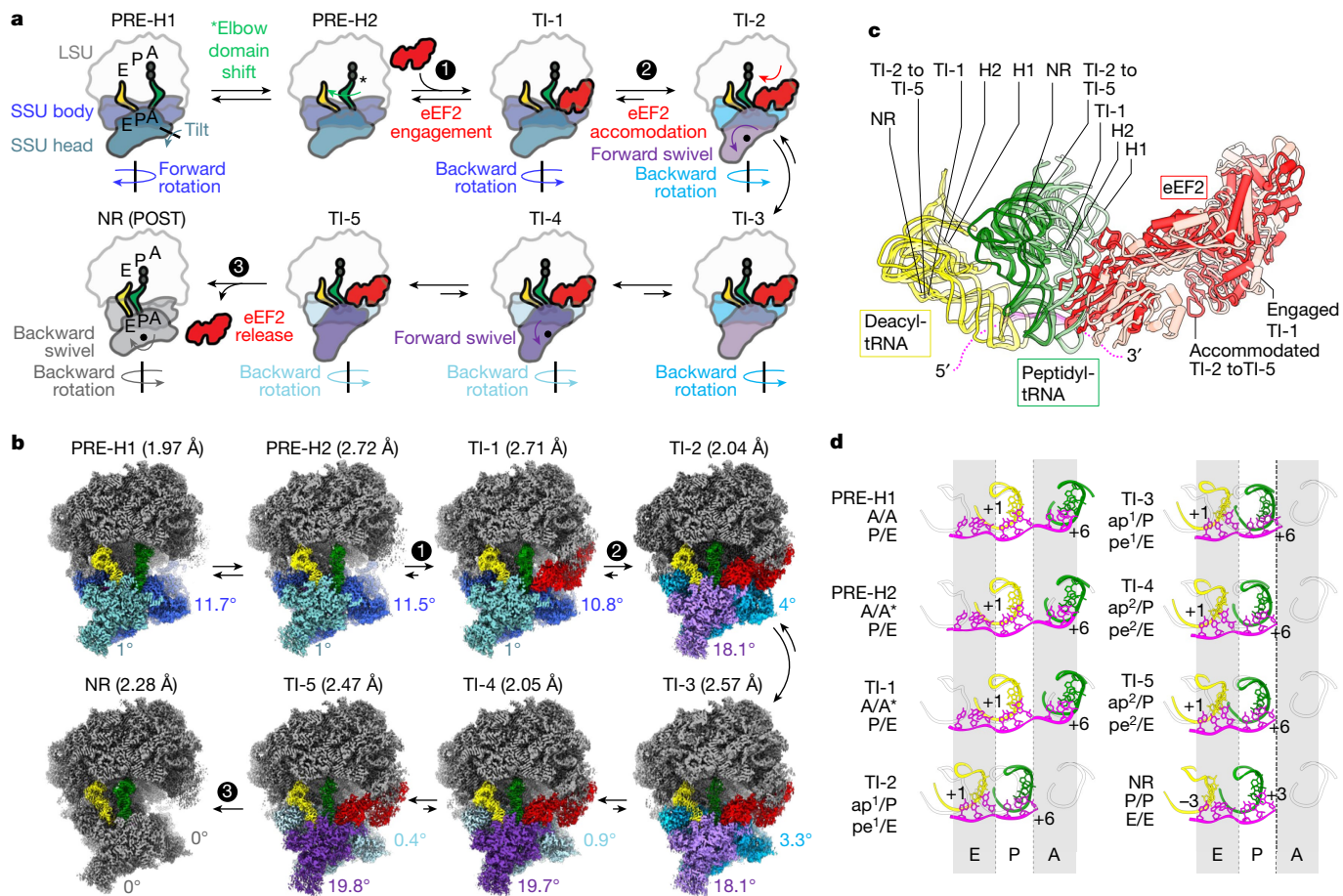


**Fig. 1 | Overview of eukaryotic ribosome TIs solved by cryo-EM. a**, A schematic representation of eukaryotic translocation based on high-resolution cryo-EM reconstructions of elongating 80S ribosomal complexes reported in the current study. eEF2-catalysed displacement of peptidyl- (green) and deacyl-tRNAs (yellow) from A to P and P to E sites, respectively, is associated with SSU body domain back rotation (dark blue to grey), and SSU head domain forward (cadet blue to violet) and backward swivelling (violet to grey). eEF2 is depicted in red. LSU is shown in grey and dipeptide in dark grey. **b**, An overview of reported

resolutions and cryo-EM maps, coloured as in a. **c**, LSU alignment shows tRNA translocation trajectories from PRE-H1 to NR depicted by light-to-dark palettes. TI-1 shows eEF2 in the recruitment phase (pink), whereas late TIs TI-2 to TI-5 reflect its fully accommodated state on the ribosome, for example, TI-5 (red). mRNA is shown in magenta. **d**, Codon–anticodon duplex advancement shown relative to PRE-H1 (A-site) and NR states (P and E sites). Alignment is performed on the SSU body domain.

state of translocation shows how elements of the mRNA–tRNA<sub>2</sub>-growing peptide module are displaced over distances of roughly 30 to 50 Å and reach a close-to-final position of translocation. Moreover, the early translocation states presented hereinafter demonstrate how the eukaryotic translocase eEF2 engages spontaneously occurring, fully rotated ribosomal conformations<sup>21</sup>, while promoting peptidyl-tRNA translocation once it is fully accommodated on 80S. We describe the mechanism of maintenance of the eukaryotic translational reading frame on the atomic level, showing how eukaryote-specific elements of the 80S ribosome, eEF2 and tRNAs, undergo large-scale molecular rearrangements to safeguard the mRNA reading frame from early eEF2 translocase accommodation until the very late stages of the process.

## Eukaryotic TIs

To visualize intermediates of the eukaryotic 80S ribosome translocation, we prepared translocating *S. cerevisiae* 80S ribosome complexes in vitro, using purified components, including naturally occurring *S. cerevisiae* eEF2. In the first set of experiments, complexes were prepared with the non-hydrolysable GTP analogue, GMPPCP, whereas in the second and third sets of experiments, the reaction mixture contained eEF2-binding translation inhibitor sordarin<sup>22</sup> and either GMP-PCP or GTP (Methods). All three reaction mixtures were subjected to

single-particle cryo-EM analysis that yielded an ensemble of nine distinct reconstructions of *S. cerevisiae* 80S ribosome bound to the complete mRNA–tRNA<sub>2</sub> module (39-nucleotide mRNA, fMet-Phe-N-tRNA<sup>Phe</sup> and deacyl-tRNA<sup>fMet</sup>). Seven of these contained *S. cerevisiae* eEF2 bound to the ribosome, respectively representing genuine eukaryotic 80S ribosome TIs (Fig. 1a,b, Extended Data Tables 1 and 2 and Supplementary Table 1). The tenth reconstruction resulted in a non-rotated (NR) state of *S. cerevisiae* 80S ribosome bound to mRNA, fMet-tRNA<sup>fMet</sup> and tRNA<sup>fMet</sup>. Altogether, these structures reflect rotational motions of the 40S small ribosomal subunit (SSU) from 0° to 11.7° relative to the 60S large subunit (LSU), SSU head swivelling from 0° to 19.8°, as well as tRNA translocation trajectories accompanied by rearrangements of several intersubunit bridges and the L1 stalk (Fig. 1a–d, Extended Data Figs. 1 and 2 and Supplementary Figs. 1 and 2a–d).

The most pronounced intersubunit rotation of roughly 12° was observed in pretranslocation substrates, referred to as the PRE-translocation-hybrid 1 (PRE-H1) and PRE-translocation-hybrid 2 (PRE-H2) complexes. These two early-stage complexes showed densities for peptidyl-tRNA in classical (A/A or A/A\*) and deacyl-tRNA in hybrid P/E states (Fig. 1b and Supplementary Fig. 1). As such, the two states, determined at 1.97 and 2.72 Å, respectively, precede eEF2 recruitment on 80S and highlight a considerable shift of roughly 23 Å that the elbow of peptidyl-tRNA performs in its transition from A/A in PRE-H1, to

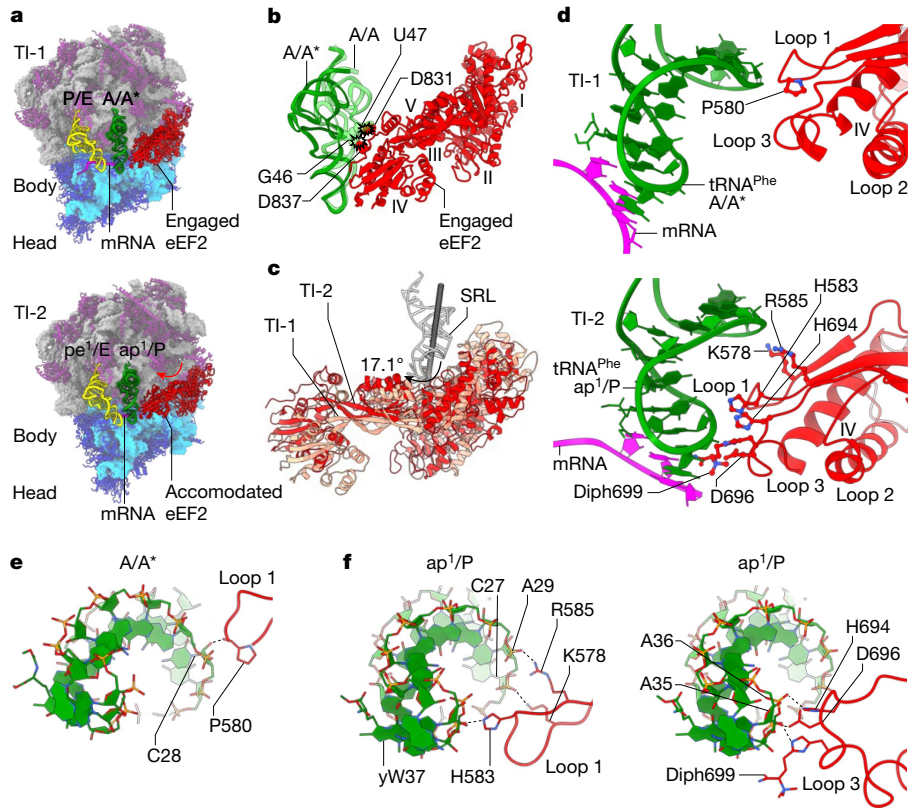


**Fig. 2 | eEF2 accommodation on the 80S ribosome and interactions of domain IV with ASL of peptidyl-tRNA in TI-1 and TI-2.** **a**, Overview of TI-1 (top) and TI-2 (bottom) with peptidyl- (green) and deacyl-tRNAs (yellow), eEF2 (red) and mRNA (magenta). eEF2 accommodation on the 80S ribosome (red arrow) occurs as tRNAs advance from the hybrid A/A\*-P/E to the chimeric ap<sup>1</sup>/P-pe<sup>1</sup>/E state. **b**, Shift of the peptidyl-tRNA elbow domain from A/A (light green) to A/A\* (green) is required for eEF2 engagement on the 80S ribosome. Clashing residues of

peptidyl-tRNA in the classical A/A state and eEF2 domain IV are shown as ball models. **c**, Rotation of eEF2 around the SRL on its transition from the engaged to the accommodated state on the 80S ribosome. **d**, Residues of eEF2 domain IV stabilizing the ASL of peptidyl-tRNA in TI-1 (top) and in TI-2 (bottom). **e,f**, Per-loop interactions of eEF2 domain IV with ASLs of peptidyl-tRNA in TI-1 (e) and TI-2 (f).

A/A\* in PRE-H2 (Supplementary Fig. 2b,c), confirming that tRNA acceptor arm movements can be uncoupled<sup>7,23,24</sup>. The NR complex (2.28 Å) has a non-swivelled head domain with tRNAs that occupy classical P/P and E/E states (Fig. 1a,b, Extended Data Fig. 1 and Supplementary Fig. 1). Although no interactions between mRNA E-codon and tRNA<sup>fMet</sup> anticodon were found in NR, the latter shows final positions of tRNA translocation and thus reflects a posttranslocation state (POST).

TI-1 to TI-5 were determined in the presence of sordarin-bound native *S. cerevisiae* eEF2 (2.04–2.71 Å), whereas TI-1\* and TI-4\* complexes were reconstructed in the absence of the inhibitor (Fig. 1a,b, Extended Data Tables 1 and 2 and Supplementary Table 1). TI-1, TI-1\*, TI-3 and TI-4\* were captured by GMPPCP, whereas TI-2, TI-4 and TI-5 were obtained from a single set of conditions in the presence of GTP and showed density for its hydrolysed GDP form. Furthermore, we observed further density in TI-4 corresponding to inorganic phosphate, Pi (Extended Data Fig. 3). The sequence of translocation events was reconstructed on the basis of observed conformations of SSU domains (body and head rotation) and the exact positions of tRNAs and the L1 stalk (Extended Data Fig. 1, Supplementary Figs. 1 and 2a–d and Supplementary Videos 1 and 2). Accordingly, TI-1 was defined as the earliest, whereas TI-5 represented the latest intermediate of eukaryotic translocation.

TI-1 and TI-1\* are visualized structures of an early eukaryotic ribosome translocation assembly, reflecting eEF2 recruitment events on 80S. Translocase recruitment is accompanied by the opening of the SSU shoulder domain, whereas fMet-Phe-N-tRNA and deacyl-tRNA<sup>fMet</sup> maintain the A/A\* and P/E configurations, respectively (Extended Data Fig. 1 and Supplementary Fig. 1). Moreover, during early translocation events (PRE-H1, PRE-H2 and TI-1, TI-1\*), the SSU head domain maintains

a tilted position of roughly 1° relative to the body (Extended Data Fig. 1). Hence, the head domain probably acts as the main ligand anchor, modulating the progression of tRNA anticodons. The importance of the head domain for tRNA translocation is further corroborated by a recent X-ray structure of an early intermediate state of eukaryotic translocation<sup>3</sup>. In this structure, eEF2 is fully accommodated, while the SSU body is still in a highly rotated state (9.5°); however, its SSU head domain has swivelled forward by 13°, coinciding with a major tRNA advancement.

During transitions from TI-2 to TI-5, 80S undergoes substantial large-scale conformational changes, in which the SSU body domain rotates backwards, being only 0.4° away (TI-5) from the final NR position, while the SSU head domain performs forward rotation of up to 19.8° (Extended Data Fig. 1). Accommodation of eEF2 on 80S, as observed from TI-1 to TI-2 (Fig. 2a), coincides with further SSU shoulder domain opening. Then, as codon–anticodon duplexes undergo modest advancement from TI-2 to TI-5 (Fig. 1d), the mRNA–tRNA<sub>2</sub> module remains in the chimeric state (Extended Data Fig. 2 and Supplementary Fig. 1). For instance, TI-2 and TI-3 states can be considered as ‘overlapping’, however, even though GTP hydrolysis had already occurred in TI-2, TI-3 was considered more advanced because the SSU body is more back rotated. Despite only a minor codon–anticodon advancement in late translocation, 80S undergoes substantial large-scale conformational changes in terms of SSU body back rotation and SSU head forward swivelling (Extended Data Fig. 1).

As expected, the final product of translocation—in which eEF2 would have dissociated from the 80S ribosome complex, and fMet-Phe-N-tRNA<sup>fMet</sup> and deacyl-tRNA<sup>fMet</sup> reached P/P and E/E positions, respectively—was not observed in any of the assayed in vitro

conditions. This confirms that the translocation process cannot be fully accomplished in the absence of GTP hydrolysis<sup>25</sup> or in the presence of sordarin<sup>22</sup>. Thus, our study supports the proposal that the elongating complex can reach a close-to-final state in a single round of translocation with no requirements for energy coming directly from GTP hydrolysis<sup>26</sup>. Analogously, final translocation events, including notably eEF2 dissociation, would therefore require the hydrolysed, GDP, form<sup>25</sup>. Ultimately, the translocase is most likely to guard against the slippage of the translational reading frame, whereas the principal role of GTP hydrolysis is to ensure eEF2 will not be released from the ribosome before completion of the translocation cycle<sup>4,25,27</sup>.

## eEF2 engagement and mRNA-tRNA<sub>2</sub> movement

Early TIs TI-1 and TI-1\* show eEF2 binding to a fully rotated hybrid intermediate ribosome captured in a conformation analogous to PRE-H2 (Fig. 1a,b and Supplementary Fig. 1). Displacement of the elbow domain of peptidyl-tRNA, which prevents the collision with domain IV of eEF2 (Fig. 2b), as well as the movement of the acceptor stem of deacyl-tRNA from P/P to P/E, demonstrate that PRE-H2 represents an authentic TI, in which acceptor stems of tRNAs had largely translocated on the LSU. This step occurs spontaneously, in the absence of both eEF2 and GTP, and can be reversible<sup>28</sup>. The TI-1 state is captured during eEF2 recruitment on 80S, with domains I and V bound to the universally conserved sarcin–ricin loop (SRL) of 25S rRNA (Fig. 2c and Extended Data Fig. 4a–d). Moreover, domain I is accommodated on uL6, domain V is in contact with uL11 and domain IV is found between the SSU shoulder and head domains. The TI-1 structure also shows eukaryote-specific points of contact between eEF2 domains I and II and SSU proteins eS6 and eS24 (Extended Data Fig. 4e). In addition, the lysine-rich loop 1 of domain IV forms initial contacts with the peptidyl-tRNA anticodon-stem loop (ASL), notably through a hydrogen bond with proline residue 580 (Fig. 2d,e). Although the interaction is not side-chain specific, it points to the fundamental importance of proline geometry for domain IV conformation in the context of translocation accuracy. Indeed, single-point mutation of proline 580 to histidine increases the rate of frameshifting events in yeast, whereas the equivalent P596H in human eEF2 is associated with human neurodegeneration phenotypes, notably autosomal dominant spinocerebellar ataxias<sup>29</sup>.

During progression to TI-2, eEF2 undergoes rotation-like movement by roughly 17° around SRL, and ultimately, accommodates on 80S (Fig. 2c). In the transition from TI-1 to TI-2, unlocking of the decoding centre enables eEF2 domain IV to move into the A-site by roughly 19 Å and engage in direct interactions with the minor groove of the codon–anticodon duplex formed by peptidyl-tRNA and the A-codon (Figs. 2f and 3a,b and Supplementary Video 3). Full accommodation of eEF2 occurs together with further SSU back rotation (Figs. 1a,b and 2a,c and Extended Data Fig. 1). These observations further suggest that unlocking of the eukaryotic ribosome decoding centre occurs during the transition from TI-1 to the early translocation state characterized by the recent crystal structure of eukaryotic *S. cerevisiae* 80S ribosome<sup>3</sup>. Disruption of minor groove interactions between rRNA elements of the decoding centre and the codon–anticodon duplex in the SSU A-site presents a rate-limiting step in enzymatic translocation<sup>30</sup>. On sequential transitions from TI-2 to TI-5, accompanied by further reverse rotation of the SSU body and forward swivelling of the head, the mRNA-tRNA<sub>2</sub> cargo reaches its close-to-final position of translocation, while eEF2 domain IV conserves its overall conformation and position on the SSU (Extended Data Figs. 2 and 5a–c and Supplementary Fig. 1). Furthermore, structures of TI-1 and TI-3 obtained in the presence of GMPPCP showed that abrogation of GTP hydrolysis does not prevent translocation from reaching a late intermediate state (Extended Data Figs. 2 and 3 and Supplementary Fig. 1). Therefore, eEF2 contributes to translocation most likely by preventing reverse rotation of the

SSU head domain, acting as a molecular ‘doorstop’<sup>3,4</sup> (Supplementary Video 4).

Although we observed gradual dissociation of eEF2 from 80S during transitions from TI-2 to TI-5 (Extended Data Fig. 4b–d), contacts between eEF2 domain IV and peptidyl-tRNA were maintained (Fig. 2d–f and Extended Data Fig. 5b). More importantly, eEF2 contributes substantially to the overall stability of the mRNA-tRNA<sub>2</sub> module, with an extra contact area of roughly 430 Å<sup>2</sup> in TI-2, TI-3 and TI-4. As such, it accounts for roughly 25% of the total contact area found to preserve the integrity of codon–anticodon duplexes, including tRNA ASLs. Our data suggest that codon–anticodon integrity is maintained until the very late stages of the translocation process, pointing to the possible existence of accuracy control mechanisms, not only on decoding but throughout the elongation cycle.

## mRNA reading frame and eEF2 domain IV

Our high-resolution structures show an intricate network of interactions preventing the slippage of the translational reading frame (Fig. 3a). First, as eEF2 is recruited on the hybrid 80S complex and TI-1 is formed, the codon–anticodon duplex of peptidyl-tRNA remains locked in the decoding centre, as observed in PRE-H1/PRE-H2, while the stem of peptidyl-tRNA ASL gains extra stability from domain IV of the not-fully accommodated eEF2 (Fig. 2d,e). In the decoding centre, the codon–anticodon duplex is secured by a highly ordered network of interactions, largely resembling the one previously described in prokaryotes<sup>31</sup>. However, we observed more interactions with the eukaryote-specific glutamine residue 63 of the conserved uS12 protein (Fig. 3a). Then, on transition from TI-1 to TI-2 and full eEF2 accommodation, the tRNA-like domain IV of eEF2 establishes an intensive network of interactions with the codon–anticodon duplex, in which diphthamide forms a total of three hydrogen bonds with the second base pair (BP2), involving both codon and anticodon nucleotides (Fig. 3a,b). A similar pattern of interactions, although with further interactions with BP1, was recently described in a TI trapped presumably at a state between TI-1 and TI-2<sup>3</sup>. Next, reconstructions of TI-3 and TI-4 suggest that the interaction network of diphthamide undergoes remodelling to include an extra contact with the third codon nucleotide, possibly by means of amide O-protonation. Finally, in TI-5, diphthamide re-establishes the interaction network with only the second codon nucleotide. This suggests that diphthamide acts by maintaining the interaction with BP2 throughout translocation, while transiently probing BP1 during early<sup>3</sup> translocation and BP3 during late translocation. Stabilization of the codon–anticodon duplex is further ensured by histidine 583 of eEF2 domain IV, found to interact with the phosphate moiety of wybutoxine 37 of tRNA<sup>Phe</sup> (Fig. 2f) from the early<sup>3</sup> to the late state of almost accomplished translocation (TI-5). In addition to the stabilizing effect of eEF2, the codon–anticodon duplex is also secured by RNA nucleotides of the SSU body domain (Fig. 3a). Our cryo-EM data also show that BP2 gains more stabilization in TI-3 onwards through an extra hydrogen bond with the ribosomal residue U1761. Moreover, wobble BP geometry in TI-4 and TI-5 is further secured by a hydrogen bond with Cm1639, which complements BP3 interacting counterparts C1637, G1638 and C1640 preserved from TI-2. Altogether, these interactions mimic the stabilizing effect of the decoding centre observed in TI-1. Ultimately, the sterically constrained environment imposed predominantly on BP2 through the arrangement of diphthamide and domain IV residues suggests that the role of eEF2 is not only to stabilize correct Watson–Crick codon–anticodon interactions but also to contribute to tRNA discrimination during translocation (Fig. 3c,d). By probing the minor groove of the peptidyl-tRNA codon–anticodon duplex, eEF2 could uncover near-cognate peptidyl-tRNA paired to the codon by non-canonical Watson–Crick interactions and trigger dissociation of erroneous peptidyl-tRNA from the eukaryotic ribosome<sup>32</sup>.

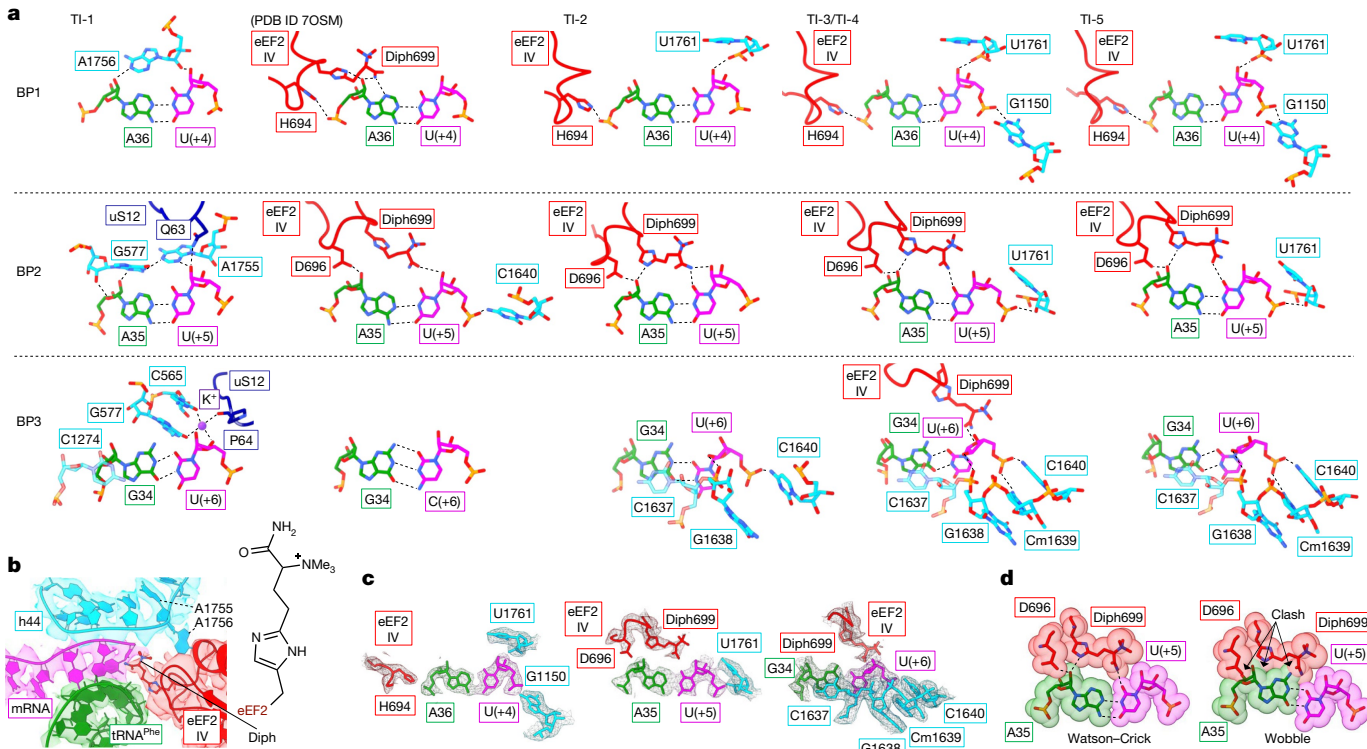


**Fig. 3 | Role of diphthamide in peptidyl-tRNA codon–anticodon stabilization.** **a**, Interactions of codon–anticodon BPs with residues of eEF2 domain IV (red), 18S rRNA (light blue) and the SSU protein uS12 (dark blue) observed in TI-1 to TI-5 and in the previously reported early TI, PDB ID 7OSM. Conserved decoding nucleotides of TI-1 are in the fully locked conformation. Diphthamide stabilizes the second codon–anticodon BP in late TIs TI-2 to TI-5 and senses the third BP in TI-3 and TI-4. Top, middle and bottom panels correspond to first (BP1), second (BP2) and third (BP3) BPs, respectively. **b**, Close-up view of hypermodified

residue diphthamide (Diph) of eEF2 domain IV (red) lying in the vicinity of the SSU helix 44 (light blue) and stabilizing the UUU codon of mRNA (magenta) and the GAA anticodon of fMet-Phe-N-tRNA<sup>Phe</sup> (green), as observed in TI-2. Unfiltered, unsharpened density is contoured at  $\sigma = 3$ . **c**, Examples of cryo-EM density for BP1–BP3 and their interacting counterparts in the TI-4 complex shown at  $\sigma = 3$ . **d**, Diphthamide and aspartate residues of eEF2 domain IV impose steric restraints to the second codon–anticodon BP and restrict wobble geometry (for example, TI-4) (Supplementary Video 3).

## Ribosome mRNA–tRNA interactions

The most expanded interaction networks between mRNA and the eukaryotic elongating ribosome were observed in hybrid and TI-1 states (for example, PRE-H1 in Extended Data Fig. 6a,b), when A-tRNA binding to the NR complex led to the narrowing of the downstream mRNA tunnel, as shown in the bacterial ribosome<sup>33</sup>, while the SSU head domain remained unrotated. mRNA is found to interact with uS12 and several 18S nucleotides in a base-non-specific manner (Extended Data Fig. 6c). All interacting elements are conserved from prokaryotes, except the eukaryote-specific Gln63 of uS12. The transition from TI-1 to subsequent late TIs leads to simultaneous disruption of the pretranslocation arrangement and formation of new posttranslocation interactions of peptidyl- and deacyl-tRNA ASLs with the SSU body domain (Fig. 4a–d). Unlike deacyl-tRNA, peptidyl-tRNA ASL interacts primarily with the SSU body rather than the head domain. This principally arises from the interactions with decoding nucleotides in TI-1 (Fig. 3a) and hybrid states. During late translocation (from TI-2 to TI-5), a preserved set of SSU body nucleotides ensures both the advancement of peptidyl-tRNA ASL through chimeric states (for example, TI-4 in Fig. 4c) and the final delivery to the classical state in NR, whereas deacyl-tRNA is almost exclusively ‘guided’ by the SSU head domain (Fig. 4c,d). Ultimately, as deacyl-tRNA reaches the classical E-site, the SSU head domain residues disengage from its ASL as a result of head domain back-swivelling to the classical NR state and restore the complete P-site setup around peptidyl-tRNA (Fig. 4d). Subsequent disruption of these interactions may be the main energy barrier to the rate-limiting step of unlocking, which is to be solved by eEF2. Indeed, following the unlocking event, eEF2

domain IV mimics the effect of decoding nucleotides to maintain the stability of weak A-codon–anticodon pairing of peptidyl-tRNA and prevent the loss of the reading frame during translocation (Figs. 3a and 4a–d).

## Eukaryote-specific RNA modifications

Here, 1-methyl-3- $\alpha$ -amino- $\alpha$ -carboxyl-propyl pseudouridine 1,191 ( $m^1\text{acp}^3\Psi1191$ ) is the only hypermodification identified in *S. cerevisiae* rRNA. This heavily modified uridine<sup>34</sup>, reported in the hairpin loop of the universally conserved helix 31 of 18S rRNA, lies at the interface of SSU head and body domains, and is known to participate in the architecture of the peptidyl-tRNA site<sup>35,36</sup> (Fig. 5a). The central importance of  $m^1\text{acp}^3\Psi1191$  is underlined by the fact that its loss (hypo-modification) is associated with the proliferation of colorectal cancer cells<sup>37</sup>. In the classical (NR) state, this hypermodification interacts with the first anticodon nucleotide of the P-site tRNA while forming a hydrogen bond with C1637 of the SSU body. This SSU head-to-body contact at positions 1,191–1,637 is then maintained during the transition to the rotated state (Fig. 5a). Despite its subsequent disruption due to eEF2 binding and forward head swivelling-associated translocation of P-site tRNA,  $m^1\text{acp}^3\Psi1191$  maintains the interaction with tRNA and guides the ASL to the E-site while covering a distance of roughly 11 Å. Finally, as deacyl-tRNA reaches its final position and the head swivels backwards,  $m^1\text{acp}^3\Psi1191$  releases E-site tRNA and immediately reaches to the next P-site tRNA ready to engage in the upcoming step of translocation (Fig. 5a and Supplementary Video 5).

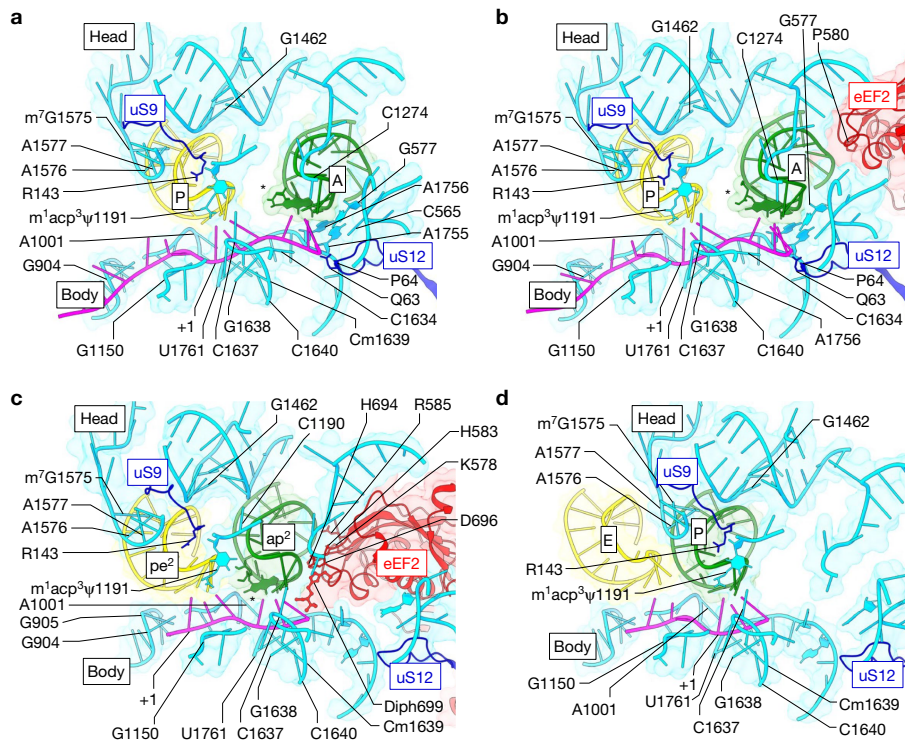


**Fig. 4 | mRNA–tRNA interactions with the SSU of the eukaryotic ribosome at different elongation states.** **a–d**, Interactions of mRNA (magenta) and ASLs of peptidyl-tRNAs (green) and deacyl-tRNAs (yellow) with domain IV of eEF2 (red) and SSU body and head domains (18S in light blue and SSU proteins in dark blue).

Movement of the mRNA–tRNA<sub>A</sub> module is shown for PRE-H1 (**a**), for TI-1 (**b**), for TI-4 (**c**) and for NR (**d**). Annotations are shown only for interacting residues. tRNA<sup>Phe</sup> hypermodification wybutosine (yW) at position 37 is marked with an asterisk.

Our structures also showed further stabilization of codon–anticodon pairing in which the wyosine moiety of the hypermodified wybutosine 37 of *S. cerevisiae* tRNA<sup>Phe</sup> (yW37) cross-strand stacks with the first codon nucleoside paired to peptidyl-tRNA<sup>Phe</sup> (Fig. 5b). As translocation reaches the late states, tighter compactness of the peptidyl-tRNA ASL can be observed. Wybutosine modulates this compactness by protruding further into the interior of the ASL and directly interacting with U32, which decreases the conformational flexibility of the anticodon loop<sup>38</sup>. Overall, these findings substantiate previous studies that showed that both the absence of yW37 and its alterations increased the ribosomal frameshifting frequency<sup>39</sup> while being linked to a lower survival of patients with cancer<sup>40</sup>.

### Sordarin action and eEF2 dissociation

Reconstructions of TI-1, TI-2, TI-3, TI-4 and TI-5 showed more density at the interface of eEF2 domains III and V corresponding to sordarin<sup>41</sup> (Extended Data Fig. 7a–j). Global alignments of ribosome-bound eEF2 in early and late states of translocation suggest that the presence of sordarin has unsubstantial effects on the overall conformation of eEF2 (ref. 5) and, more importantly, has little-to-no effect either on the position or the conformation of eEF2 domains I and IV relative to the 80S ribosome (Extended Data Fig. 7a–c). However, eEF2 domain III alignment indicates that sordarin bridges the domain III–V interface (Extended Data Fig. 7d–i). Consequently, the mechanism of sordarin-induced eEF2 stalling on the 80S ribosome most probably proceeds by domain interface remodelling. Late translocation (TI-2 to TI-5) is associated with a stepwise decrease of the overall contact area between eEF2 and both the full 80S and the individual subunits (Extended Data Fig. 4b–d), however, the interactions of eEF2 domain II with the SSU shoulder protein uS12 expand as the entire SSU body domain rotates backwards (Extended Data Fig. 1 and 8a,b). Structural

analyses corroborate these findings and show that uS12 prevents further progression of eEF2 on the SSU (Extended Data Fig. 8a). The interactions between eEF2 domain III and uS12 follow the overall decreasing trend of eEF2/80S contacts only until the penultimate translocation state TI-4, from where the contact area between domain III and uS12 increases (Extended Data Fig. 4b–d and 8b). Indeed, our structures show that the  $\alpha$ -helix A of domain III swings in the direction of domain V, which in turn can trigger eEF2 dissociation from the translocating ribosomal assembly, as proposed in earlier works on non-canonical IRES-mediated translocation<sup>42</sup>. Recently, Carbone et al. observed a similar trend in EF-G domain III rearrangement relative to uS12 in a late bacterial translocation state in which EF-G dissociation had already commenced and the GTPase domain had unbound from the ribosome<sup>7</sup>. We propose that the mechanism of sordarin action most probably consists of blocking the full remodelling of eEF2 domain III with respect to domain V, which possibly leads to eEF2 stalling on 80S and, ultimately, late translocation arrest. We cannot exclude that sordarin action on eEF2 might inhibit conformational changes of the switch loop 2 (sw2) through a similar mechanism proposed for argyrin B (ArgB)<sup>43</sup> (Extended Data Fig. 7g–i). As for ArgB, sordarin seems to indirectly prevent sw2 remodelling, which is expected to be necessary for eEF2 dissociation. In comparison, fusidic acid, a bacterial EF-G-targeting antibiotic, binds to a distinct site vacated by the released inorganic phosphate and, unlike sordarin and ArgB, blocks eEF2 by directly stabilizing the GTP-like conformation of sw2 (ref. 6). However, in contrast to fusidic acid and ArgB that trap the mid-TI INT2 (refs. 6,43), sordarin allows the eukaryotic translocating assembly to reach the late intermediate state TI-5. Finally, our TI-4 showed density for inorganic phosphate, suggesting that in the presence of sordarin, and without phosphate release or domain IV remodelling, translocation is almost fully accomplished and a late chimeric state can be formed.

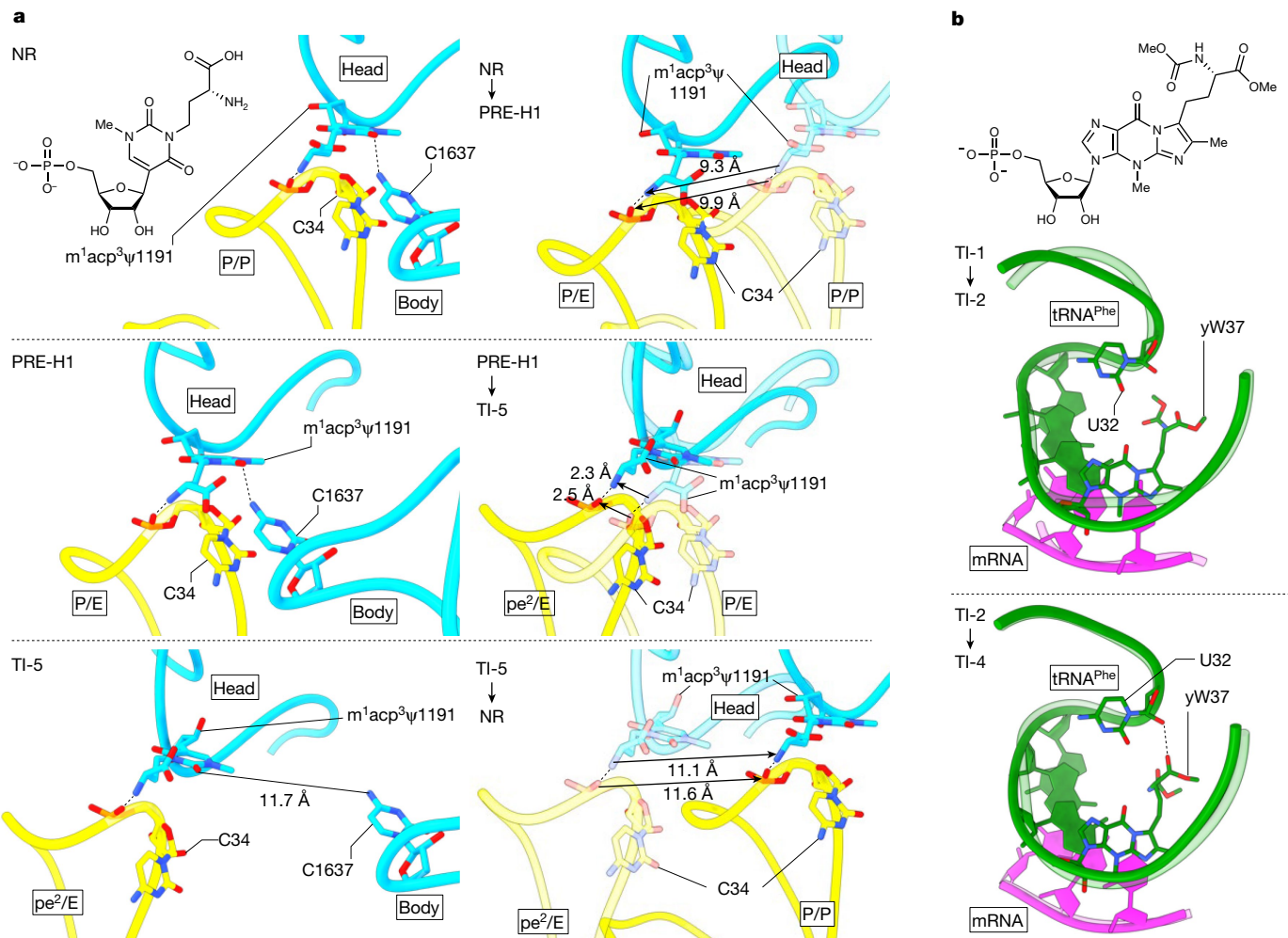


**Fig. 5 | Role of *S. cerevisiae* hypermodifications m<sup>1</sup>acp<sup>3</sup>Ψ1191 of 18S and wybutoxine (yW37) of tRNA<sup>Phe</sup>.** a, Base-unspecific hydrogen bond interactions between hypermodified 1-methyl-3-α-amino-α-carboxyl-propyl pseudouridine (m<sup>1</sup>acp<sup>3</sup>Ψ1191) and the first anticodon nucleotide C34 of deacyl-tRNA<sup>fMet</sup> (yellow) are shown for NR, PRE-H1 and TI-5 states (left). In NR and early TIs (for example, PRE-H1), m<sup>1</sup>acp<sup>3</sup>Ψ1191 interacts with the SSU body residue C1637, compatible with non-swivelled conformations of the SSU head. Swivelled conformations of the SSU head domain in late TIs (for example, TI-5) break the contact between m<sup>1</sup>acp<sup>3</sup>Ψ1191 and C1637. Respective transitions between NR,

PRE-H1 and TI-5 states (right) show that the m<sup>1</sup>acp<sup>3</sup>Ψ1191 platform guides deacyl-tRNA<sup>fMet</sup> anticodon translocation by fixing and moving C34 from the P towards the E site, after which the anticodon is released and the hypermodification fixes the next P-site anticodon. **b**, Bulky chain of yW37 protrudes into the ASL and forms a hydrogen bond with U32 in TI-4. ASL alignments of fMet-Phe-tRNA<sup>Phe</sup> (residues 27–43) during transitions from TI-1 to TI-2, and from TI-2 to TI-4 show intramolecular remodelling of the tRNA<sup>Phe</sup> ASL (Supplementary Video 5).

## Discussion

Here we present atomic-resolution structural information for the understanding of the mechanism of movement of the mRNA-tRNA<sub>2</sub>-growing peptide module during protein synthesis in eukaryotes. We characterize eukaryotic TIs whose existence had only been proposed on the basis of bacterial translocation but their reconstructions had never been reported. Our data describe how the eukaryotic translocase eEF2 is engaged by a spontaneously rotated 80S ribosome and reveal the importance of its contacts with coevolved eukaryote-specific SSU proteins. This study shows that the extra complexity of the eukaryotic translational apparatus, in comparison with the prokaryotic system, reflects more sophisticated and more finely regulated mechanisms of maintenance of the mRNA-tRNA<sub>2</sub> module during its translocation through the ribosome. An extensive system of eukaryote-specific rRNA and tRNA posttranscriptional modifications, together with eEF2 and its unique posttranslational modification, actively contribute to the accuracy of protein synthesis by preventing the slippage of the translational reading frame (Supplementary Video 6).

We propose that the sterically constrained environment imposed by the eukaryote-specific posttranslational modification diphthamide, in the context of domain IV conformation, not only stabilizes correct Watson–Crick codon–anticodon interactions but may uncover the erroneous peptidyl-tRNA by probing the minor groove of the codon–anticodon duplex. Therefore, this extra proofreading mechanism that prevents incorporation of an incorrect amino acid during translocation contributes to higher accuracy of protein synthesis in eukaryotes. Our reconstructions in the presence of GMPPCP demonstrated nearly complete movement of the tRNA<sub>2</sub>-mRNA module, corroborating the model in which the translocase functions as a molecular doorstop, which uncouples the mRNA-tRNA<sub>2</sub> movement from the thermally driven back rotation of the SSU body and/or platform<sup>23,26,27,42,44,45</sup>. Hence, it seems that the primary role of GTP hydrolysis in translocation in all kingdoms of life is to establish an irreversible step that prevents translocase release until both tRNAs and mRNA have moved by one full codon. Such a mechanism would ensure productive translocation and efficient maintenance of the translational reading frame<sup>3,6,7,25</sup>.

Here we propose the mechanism of translocation inhibition by sordarin. It can bind to ribosome-associated eEF2 from the early T1-1 state and seems not to affect global eEF2 conformation or otherwise interfere with subsequent eEF2 accommodation on the ribosome. As translocation then reaches the late T1-5 state, sordarin supposedly stalls eEF2 on the ribosome by preventing domain III remodelling and ultimate dissociation from the ribosome.

Although our results provide atomic-resolution information on molecular mechanisms of eukaryotic ribosome translocation, further structural studies, including time-resolved cryo-EM and biochemical investigations of mRNA-tRNA displacement through the eukaryotic ribosome, are needed to provide full understanding of the precise timing of GTP hydrolysis and Pi release, as well as translocation proofreading mechanisms that ensure accurate protein synthesis in eukaryotes.

## Online content

Any methods, additional references, Nature Portfolio reporting summaries, source data, extended data, supplementary information, acknowledgements, peer review information; details of author contributions and competing interests; and statements of data and code availability are available at <https://doi.org/10.1038/s41586-023-06780-4>.

1. Ortiz, P. A., Ulloque, R., Kihara, G. K., Zheng, H. & Kinzy, T. G. Translation elongation factor 2 anticodon mimicry domain mutants affect fidelity and diphtheria toxin resistance. *J. Biol. Chem.* **281**, 32639–32648 (2006).
2. Liu, S. et al. Diphthamide modification on eukaryotic elongation factor 2 is needed to assure fidelity of mRNA translation and mouse development. *Proc. Natl. Acad. Sci. USA* **109**, 13817–13822 (2012).
3. Djumagulov, M. et al. Accuracy mechanism of eukaryotic ribosome translocation. *Nature* **600**, 543–546 (2021).
4. Flis, J. et al. tRNA translocation by the eukaryotic 80S ribosome and the impact of GTP hydrolysis. *Cell Rep.* **25**, 2676–2688 e2677 (2018).
5. Taylor, D. J. et al. Structures of modified eEF2 80S ribosome complexes reveal the role of GTP hydrolysis in translocation. *EMBO J.* **26**, 2421–2431 (2007).
6. Rundlet, E. J. et al. Structural basis of early translocation events on the ribosome. *Nature* **595**, 741–745 (2021).
7. Carbone, C. E. et al. Time-resolved cryo-EM visualizes ribosomal translocation with EF-G and GTP. *Nat. Commun.* **12**, 7236 (2021).
8. Petrychenko, V. et al. Structural mechanism of GTPase-powered ribosome-tRNA movement. *Nat. Commun.* **12**, 5933 (2021).
9. Zhou, J., Lancaster, L., Donohue, J. P. & Noller, H. F. How the ribosome hands the A-site tRNA to the P site during EF-G-catalyzed translocation. *Science* **345**, 1188–1191 (2014).
10. Zhou, J., Lancaster, L., Donohue, J. P. & Noller, H. F. Crystal structures of EF-G-ribosome complexes trapped in intermediate states of translocation. *Science* **340**, 1236086 (2013).
11. Ramrath, D. J. et al. Visualization of two transfer RNAs trapped in transit during elongation factor G-mediated translocation. *Proc. Natl. Acad. Sci. USA* **110**, 20964–20969 (2013).
12. Melnikov, S. et al. One core, two shells: bacterial and eukaryotic ribosomes. *Nat. Struct. Mol. Biol.* **19**, 560–567 (2012).
13. Budkevich, T. V. et al. Regulation of the mammalian elongation cycle by subunit rolling: a eukaryotic-specific ribosome rearrangement. *Cell* **158**, 121–131 (2014).
14. Dever, T. E., Dinman, J. D. & Green, R. Translation elongation and recoding in eukaryotes. *Cold Spring Harb. Perspect. Biol.* **10**, a032649 (2018).
15. Iglewski, B. H. & Kabat, D. NAD-dependent inhibition of protein synthesis by *Pseudomonas aeruginosa* toxin. *Proc. Natl. Acad. Sci. USA* **72**, 2284–2288 (1975).
16. Lee, H. & Iglewski, W. J. Cellular ADP-ribosyltransferase with the same mechanism of action as diphtheria toxin and *Pseudomonas* toxin A. *Proc. Natl. Acad. Sci. USA* **81**, 2703–2707 (1984).
17. Arguelles, S., Camandola, S., Cutler, R. G., Ayala, A. & Mattson, M. P. Elongation factor 2 diphthamide is critical for translation of two IRES-dependent protein targets, XIAP and FGF2, under oxidative stress conditions. *Free Radic. Biol. Med.* **67**, 131–138 (2014).
18. Hawer, H. et al. Diphthamide-deficiency syndrome: a novel human developmental disorder and ribosomopathy. *Eur. J. Hum. Genet.* **28**, 1497–1508 (2020).
19. Shankar, S. P. et al. A novel DPH5-related diphthamide-deficiency syndrome causing embryonic lethality or profound neurodevelopmental disorder. *Genet. Med.* **24**, 1567–1582 (2022).
20. Stahl, S. et al. Loss of diphthamide pre-activates NF-kappaB and death receptor pathways and renders MCF7 cells hypersensitive to tumor necrosis factor. *Proc. Natl. Acad. Sci. USA* **112**, 10732–10737 (2015).
21. Chen, J., Tsai, A., O’Leary, S. E., Petrov, A. & Puglisi, J. D. Unraveling the dynamics of ribosome translocation. *Curr. Opin. Struct. Biol.* **22**, 804–814 (2012).
22. Justice, M. C. et al. Elongation factor 2 as a novel target for selective inhibition of fungal protein synthesis. *J. Biol. Chem.* **273**, 3148–3151 (1998).
23. Munro, J. B., Altman, R. B., O’Connor, N. & Blanchard, S. C. Identification of two distinct hybrid state intermediates on the ribosome. *Mol. Cell* **25**, 505–517 (2007).
24. Budkevich, T. et al. Structure and dynamics of the mammalian ribosomal pretranslocation complex. *Mol. Cell* **44**, 214–224 (2011).
25. Rexroad, G., Donohue, J. P., Lancaster, L. & Noller, H. F. The role of GTP hydrolysis by EF-G in ribosomal translocation. *Proc. Natl. Acad. Sci. USA* **119**, e2212502119 (2022).
26. Inoue-Yokosawa, N., Ishikawa, C. & Kaziro, Y. The role of guanosine triphosphate in translocation reaction catalyzed by elongation factor G. *J. Biol. Chem.* **249**, 4321–4323 (1974).
27. Kaziro, Y. The role of guanosine 5'-triphosphate in polypeptide chain elongation. *Biochim. Biophys. Acta* **505**, 95–127 (1978).
28. Cornish, P. V., Ermolenko, D. N., Noller, H. F. & Ha, T. Spontaneous intersubunit rotation in single ribosomes. *Mol. Cell* **30**, 578–588 (2008).
29. Hekman, K. E. et al. A conserved eEF2 coding variant in SCA26 leads to loss of translational fidelity and increased susceptibility to proteostatic insult. *Hum. Mol. Genet.* **21**, 5472–5483 (2012).
30. Khade, P. K. & Joseph, S. Messenger RNA interactions in the decoding center control the rate of translocation. *Nat. Struct. Mol. Biol.* **18**, 1300–1302 (2011).
31. Demeshkina, N., Jenner, L., Westhof, E., Yusupov, M. & Yusupova, G. A new understanding of the decoding principle on the ribosome. *Nature* **484**, 256–259 (2012).
32. Zaher, H. S. & Green, R. Fidelity at the molecular level: lessons from protein synthesis. *Cell* **136**, 746–762 (2009).
33. Jenner, L. B., Demeshkina, N., Yusupova, G. & Yusupov, M. Structural aspects of messenger RNA reading frame maintenance by the ribosome. *Nat. Struct. Mol. Biol.* **17**, 555–560 (2010).
34. Meyer, B. et al. The Bowen-Conradi syndrome protein Nep1 (Emg1) has a dual role in eukaryotic ribosome biogenesis, as an essential assembly factor and in the methylation of Psi1191 in yeast 18S rRNA. *Nucleic Acids Res.* **39**, 1526–1537 (2011).
35. Ben-Shem, A. et al. The structure of the eukaryotic ribosome at 3.0 Å resolution. *Science* **334**, 1524–1529 (2011).
36. Ben-Shem, A., Jenner, L., Yusupova, G. & Yusupov, M. Crystal structure of the eukaryotic ribosome. *Science* **330**, 1203–1209 (2010).
37. Babaian, A. et al. Loss of m(1)acp(3)Psi ribosomal RNA modification is a major feature of cancer. *Cell Rep.* **31**, 107611 (2020).
38. Stuart, J. W., Koslap, K. M., Guenther, R. & Agris, P. F. Naturally-occurring modification restricts the anticodon domain conformational space of tRNA(Phe). *J. Mol. Biol.* **334**, 901–918 (2003).
39. Carlson, B. A. et al. Transfer RNA modification status influences retroviral ribosomal frameshifting. *Virology* **255**, 2–8 (1999).
40. Rossello-Tortella, M. et al. Epigenetic loss of the transfer RNA-modifying enzyme TYW2 induces ribosome frameshifts in colon cancer. *Proc. Natl. Acad. Sci. USA* **117**, 20785–20793 (2020).
41. Jorgensen, R. et al. Two crystal structures demonstrate large conformational changes in the eukaryotic ribosomal translocase. *Nat. Struct. Biol.* **10**, 379–385 (2003).
42. Murray, J. et al. Structural characterization of ribosome recruitment and translocation by type IV IRES. *eLife* **5**, e13567 (2016).
43. Wieland, M. et al. The cyclic octapeptide antibiotic argyrin B inhibits translation by trapping EF-G on the ribosome during translocation. *Proc. Natl. Acad. Sci. USA* **119**, e2114214119 (2022).
44. Pestka, S. Studies on the formation of transfer ribonucleic acid-ribosome complexes. 3. The formation of peptide bonds by ribosomes in the absence of supernatant enzymes. *J. Biol. Chem.* **243**, 2810–2820 (1968).
45. Yusupova, G. Z., Belitsina, N. V. & Spirin, A. S. Template-free ribosomal synthesis of polypeptides from aminoacyl-tRNA. Polyphenylalanine synthesis from phenylalanyl-tRNALys. *FEBS Lett.* **206**, 142–146 (1986).

**Publisher’s note** Springer Nature remains neutral with regard to jurisdictional claims in published maps and institutional affiliations.

Springer Nature or its licensor (e.g. a society or other partner) holds exclusive rights to this article under a publishing agreement with the author(s) or other rightsholder(s); author self-archiving of the accepted manuscript version of this article is solely governed by the terms of such publishing agreement and applicable law.

© The Author(s), under exclusive licence to Springer Nature Limited 2023

## Methods

### Purification of *S. cerevisiae* 80S ribosome

*S. cerevisiae* 80S ribosomes were purified from the JD1370-ΔStm1 strain<sup>46</sup> following a previously published protocol with minor modifications<sup>35</sup>. After cell disruption, ribosomes were isolated by PEG 20,000 precipitation between 4 and 8.5% w/v and purified on 15–30% w/v sucrose gradients (20 mM HEPES/KOH pH 7.5, 120 mM KCl, 10 mM MgCl<sub>2</sub>, 10% w/v sucrose, 2 mM dithiothreitol (DTT), 0.37 mM EDTA, 2.5 mM spermidine). The peak of 80S ribosomes was pooled, precipitated by PEG 20,000 and subsequently redissolved in buffer G (10 mM HEPES/KOH pH 7.5, 50 mM CH<sub>3</sub>COOK, 10 mM NH<sub>4</sub>Cl, 5 mM (CH<sub>3</sub>COO)<sub>2</sub>Mg, 2 mM DTT).

### Purification of endogenous *S. cerevisiae* eEF2

Native eEF2 was isolated from the *S. cerevisiae* JD1370-ΔStm1 strain according to a previously reported protocol<sup>47</sup> with some modifications. Following microfluidizer cell disruption and lysate dialysis, eEF2 was purified on HiLoad SP Sepharose and Q Sepharose, after which the sample was applied to a HiLoad 16/600 Superdex 200 pg gel filtration column (all from GE Healthcare). Eluted eEF2 fractions were concentrated and stored in 20 mM HEPES/KOH pH 7.5, 10% v/v glycerol, 5 mM MgCl<sub>2</sub>, 1 mM DTT, 100 mM KCl.

### Purification and aminoacylation of tRNAs

Amino-tailing of *S. cerevisiae* tRNA<sup>Phe</sup> (replacement of the 3'-terminal A76 nucleotide carrying the 3'-OH group with the one carrying 3'-NH<sub>2</sub>) was performed as previously reported<sup>48</sup> with some modifications. A mixture containing 40 μM deacylated native *S. cerevisiae* tRNA<sup>Phe</sup> (Sigma-Aldrich), 1 mM 3'-amino-3'-deoxyadenosine-5'-O-triphosphate (Biolog Life Science Institute GmbH), 1 mM sodium pyrophosphate (Sigma-Aldrich), 70 μM CCA-adding enzyme, 10 mM MgCl<sub>2</sub>, 100 mM glycine and NaOH pH 9, 1 mM DTT was incubated at 37 °C for 1 h and 20 min. The reaction was terminated by addition of EDTA to 20 mM, treated with a 1:1 phenol:chloroform mixture and precipitated with ethanol. The pellet was washed twice, dissolved in 30 μl of 10 mM HEPES/KOH pH 7.5 and purified on a Sephadex G-25 spin column (Sigma-Aldrich). The resulting, full-length, *S. cerevisiae* 3'-NH<sub>2</sub>-tRNA<sup>Phe</sup> was enzymatically acylated with phenylalanine as previously described<sup>49</sup> with minor modifications. *S. cerevisiae* Phe-N-tRNA<sup>Phe</sup> was purified on a Waters C4 column (Delta-Pak C4, 300 Å, 5 μm, 3.9 × 150 mm, 1,000–30,000, one per pack) by applying a linear ethanol gradient (as reported in ref. 50) and stored in 20 mM CH<sub>3</sub>COONH<sub>4</sub> pH 5.

Following purification of its overexpressed form, *E. coli* initiator tRNA<sup>fMet</sup> was aminoacylated and formylated according to previously published protocols<sup>51</sup>. The reaction mix was phenol extracted and the aqueous phase was applied to a TSKgel Phenyl-5PW column (Tosoh bioscience). Purified fractions of fMet-tRNA<sup>fMet</sup> were stored in 20 mM CH<sub>3</sub>COONH<sub>4</sub> pH 5.

### Formation of 80S ribosome translocation complexes

For reconstitution of translocation complexes 80S-tRNA<sub>2</sub>-mRNA-eEF2-GMPPCP or 80S-tRNA<sub>2</sub>-mRNA-eEF2-GTP, *S. cerevisiae* 80S ribosomes (2.2 μM) and 39-nucleotide-long mRNA (5'-AAAAGAAAAGAAAAGUUUUUUGAAGAAAAGAA-3', Dharmacon) (10.8 μM) were incubated at 30 °C for 10 min in 10 mM HEPES/KOH pH 7.5, 50 mM CH<sub>3</sub>COOK, 10 mM NH<sub>4</sub>Cl, 5 mM (CH<sub>3</sub>COO)<sub>2</sub>Mg, 2 mM DTT. *E. coli* fMet-tRNA<sup>fMet</sup> (10.8 μM) and *S. cerevisiae* Phe-N-tRNA<sup>Phe</sup> (10.8 μM) were then added in two steps and incubation continued for 5 and 3 min, respectively. Separately, *S. cerevisiae* eEF2 (10.8 μM) was incubated either with GMPPCP (255 μM) or GTP (255 μM) for 10 min at room temperature. Each of the two eEF2 mixtures was then added to the ribosome mix and buffer conditions were re-adjusted to 10 mM HEPES/KOH pH 7.5, 50 mM CH<sub>3</sub>COOK, 10 mM NH<sub>4</sub>Cl, 6 mM (CH<sub>3</sub>COO)<sub>2</sub>Mg and 1.25 mM DTT. Furthermore, if present, sordarin (Sigma-Aldrich)

was added at this stage to a final concentration of 100 μM. The last incubation step proceeded for another 10 min at 30 °C.

### Cryo-EM grid preparation and data collection

Following complex formation, 3 μl of sample were applied to glow-discharged Ultrathin Carbon Quantifoil R 2/2 on 300 gold mesh (Jena Bioscience) using a Mark IV Vitrobot (Thermo Fisher Scientific). Incubation of grids at 9 °C and 95% humidity lasted for 30 s and was immediately followed by blotting and flash freezing in liquid ethane, precooled to the liquid nitrogen temperature. Grid screening was performed on a 200 kV Glacios transmission electron microscope (Thermo Fisher Scientific) equipped with a K2 Summit direct electron detector (Gatan).

Single-molecule datasets were acquired at the Dubochet Center for Imaging of EPFL and the University of Lausanne (DCI-Lausanne) on a 300 kV Titan Krios G4i transmission electron microscope (Thermo Fisher Scientific) equipped with a Cold FEG emission gun, SelectrisX energy filter and a Falcon IV direct electron detector. Datasets were collected using the EPU automated software (Thermo Fisher Scientific) and a pixel size at detector of 0.450 Å per pixel (for eEF2-GMPPCP and eEF2-GTP datasets with sordarin) and 0.726 Å per pixel (for the eEF2-GMPPCP dataset without sordarin). Total electron exposure was set to 60 e<sup>-</sup>/Å<sup>2</sup> for the eEF2-GTP-sordarin dataset and 40 e<sup>-</sup>/Å<sup>2</sup> for both eEF2-GMPPCP and eEF2-GMPPCP-sordarin datasets.

### Cryo-EM data processing of the 80S-eEF2-GTP-sordarin elongation complex

Cryo-EM image processing was performed using cryoSPARC<sup>52</sup>. Raw micrographs were motion corrected, and contrast transfer function (CTF) estimation was carried out. A total of 616,978 particles were auto-picked and extracted with Fourier cropping four times (bin4 data). Several rounds of two-dimensional (2D) classification were performed, and an ab initio structure was reconstructed and used for initial three-dimensional (3D) variability analysis<sup>53</sup>. The resulting volumes were subjected to heterogeneous refinement against a total of 442,508 particles from selected 2D classes. This resulted in four structures, each representing different rotational states of the 40S subunit. Three meaningful classes were selected and subjected to further 3D variability analysis, resulting in three subclasses for each class.

The first class consisted of 170,386 particles with the fully rotated 40S subunit. Its first subclass contained both deacyl- and peptidyl-tRNAs, but no eEF2. This subpopulation was re-extracted (bin2), and homogeneous refinement yielded the PRE-H1 complex (55,455 particles). Although two other subclasses contained the elongation factor and were refined to high resolution, they were not further examined because of the absence of peptidyl-tRNA.

The second class of 133,186 particles with a semirotated 40S subunit resulted in subclasses, all of which contained deacyl- and peptidyl-tRNAs and eEF2. Particle re-extraction (bin2), followed by respective homogeneous refinements, resulted in two intermediate translocation structures, TI-2 (58,531 particles) and TI-4 (55,762 particles).

Finally, the third class with 133,186 particles and a NR 40S subunit also yielded three subclasses. The first subclass possessing only tRNAs was pooled and local refinement yielded the NR complex (21,458 particles). Two remaining subclasses contained clear density for eEF2. The meaningful class (51,517 particles) was subjected to further 3D variability analysis and a well resolved subpopulation was re-extracted (bin2) and processed by homogenous refinement that yielded the TI-5 complex (23,773 particles).

### Cryo-EM data processing of the 80S-eEF2-GMPPCP-sordarin elongation complex

Raw micrographs were motion corrected and CTF estimated<sup>52</sup>. Then, 514,460 particles were auto-picked and extracted with Fourier cropping

# Article

four times (bin4). Two rounds of 2D classification were performed, good 2D classes were selected and 393,786 particles were re-extracted. Consensus homogenous refinement was performed, and the volume was applied to 3D variability analysis<sup>33</sup>.

The class with the rotated 40S subunit (42,053 particles) was subjected to 3D variability analysis that resulted in four subclasses. Only the subclasses possessing density for both tRNAs and eEF2 were selected, particles were re-extracted (bin2) and homogenous refinement yielded the TI-1 complex (23,096 particles).

Classes with the semirotated 40S subunit were combined and run through 3D variability analysis yielding five subclasses. Three of the five subclasses showed strong density for both tRNAs and eEF2. They were pooled together, particles were re-extracted (bin2) and refined, yielding the TI-3 complex (73,086 particles).

## Cryo-EM data processing of the 80S-eEF2-GMPPCP elongation complex

Raw micrographs were motion corrected, CTF estimated, particles were auto-picked and extracted with Fourier cropping four times (bin4). Selected 2D classes yielding 561,498 particles were used to refine the initial volume. Next, particles were subjected to 3D variability analysis and separated either on the basis of 40S subunit rotation (workflow 1) or presence of strong density of tRNA and eEF2 ligands (workflow 2).

In workflow 1, the population containing rotated 40S (157,099 particles) was re-extracted (twofold binned) and subject to a new round of 3D variability analysis. One of the resulting subclasses contained deacyl- and peptidyl-tRNAs, but no elongation factor 2. Particles were re-extracted without Fourier cropping (fully unbinned, bin1) and supplied to homogenous refinement that yielded the PRE-H2 structure (68,945 particles). The second subclass with the NR 40S (118,986 particles) was re-extracted and subjected to 3D variability analysis, and only the subpopulation with strong tRNA density was pooled. Particles were then re-extracted (bin2) and applied to homogenous refinement that yielded the TI-4\* complex (41,878 particles).

In workflow 2, 276,089 particles possessing strong tRNA and eEF2 density were selected from initial 3D variability analysis. Following, two series of further 3D variability analysis, only particles with strong ligand density were pooled. This subpopulation was re-extracted (bin2) and supplied to homogenous refinement that yielded the TI-1\* complex (22,551 particles).

## Model building and refinement

Protein Data Bank (PDB) ID 7OSM was split into 60S, 40S body and head domains, eEF2 and deacyl-tRNA. Submodels were then rigid fitted into cryo-EM maps using the fitmap command in ChimeraX<sup>54,55</sup>. mRNA, peptidyl-tRNA, dipeptide, sordarin and rRNA modifications were built de novo in COOT. Several cycles of manual building in COOT and real space refinement in Phenix<sup>56,57</sup> were then performed for each model. Restraints were generated using the ELBOW algorithm integrated in the Phenix suite<sup>58</sup>.

## Model superimpositions and motion measurements

Models were superimposed using the mmaker command integrated in ChimeraX. Per-residue root-mean square deviation values for individual chains were calculated in ChimeraX using the rmsd command. The root-mean square deviation calculations of entire 40S subunits were performed in PyMOL using the colorbyrmsd script (The PyMOL Molecular Graphics System, v.2.0 Schrödinger, LLC.). Rotation measurements and axis projections were generated using the measure rotation command in ChimeraX. Contact areas were quantified by

applying the measure buriedarea command and default parameters for solvent-accessible surface calculations available through ChimeraX.

## Reporting summary

Further information on research design is available in the Nature Portfolio Reporting Summary linked to this article.

## Data availability

Atomic coordinates and cryo-EM maps generated during this study are available through the PDB and the Electron Microscopy Data bank (EMDB). The complexes have been deposited under following accession codes: PRE-H1 (8CCS, EMD-16563), PRE-H2 (8CDL, EMD-16591), TI-1 (8CF5, EMD-16616), TI-2 (8CDR, EMD-16594), TI-3 (8CG8, EMD-16634), TI-4 (8CEH, EMD-16609), TI-5 (8CIV, EMD-16684), NR (8CGN, EMD-16648), TI-1\* (8CKU, EMD-16702) and TI-4\* (8CMJ, EMD-16729).

46. Pellegrino, S. et al. Structural insights into the role of diphthamide on elongation factor 2 in mRNA reading-frame maintenance. *J. Mol. Biol.* **430**, 2677–2687 (2018).
47. Jorgensen, R., Carr-Schmid, A., Ortiz, P. A., Kinzy, T. G. & Andersen, G. R. Purification and crystallization of the yeast elongation factor eEF2. *Acta Crystallogr. D Biol. Crystallogr.* **58**, 712–715 (2002).
48. Fraser, T. H. & Rich, A. Synthesis and aminoacylation of 3'-amino-3'-deoxy transfer RNA and its activity in ribosomal protein synthesis. *Proc. Natl Acad. Sci. USA* **70**, 2671–2675 (1973).
49. Spirin, A. S., Belitsina, N. V. & Yusupova, G. Z. Ribosomal synthesis of polypeptides from aminoacyl-tRNA without polynucleotide template. *Methods Enzymol.* **164**, 631–649 (1988).
50. Mesters, J. R., Vorstenbosch, E. L. H., Deboer, A. J. & Kraal, B. Complete purification of transfer-RNA, charged or modified with hydrophobic groups, by reversed-phase high-performance liquid-chromatography on a C-4 C-18 column system. *J. Chromatogr. A* **679**, 93–98 (1994).
51. Mechulam, Y., Guillou, L., Yatime, L., Blanquet, S. & Schmitt, E. Protection-based assays to measure aminoacyl-tRNA binding to translation initiation factors. *Methods Enzymol.* **430**, 265–281 (2007).
52. Punjani, A., Rubinstein, J. L., Fleet, D. J. & Brubaker, M. A. cryoSPARC: algorithms for rapid unsupervised cryo-EM structure determination. *Nat. Methods* **14**, 290–296 (2017).
53. Punjani, A. & Fleet, D. J. 3D variability analysis: resolving continuous flexibility and discrete heterogeneity from single particle cryo-EM. *J. Struct. Biol.* **213**, 107702 (2021).
54. Goddard, T. D. et al. UCSF ChimeraX: meeting modern challenges in visualization and analysis. *Protein Sci.* **27**, 14–25 (2018).
55. Pettersen, E. F. et al. UCSF ChimeraX: structure visualization for researchers, educators, and developers. *Protein Sci.* **30**, 70–82 (2021).
56. Terwilliger, T. C. et al. Improved crystallographic models through iterated local density-guided model deformation and reciprocal-space refinement. *Acta Crystallogr. D Biol. Crystallogr.* **68**, 861–870 (2012).
57. Liebschner, D. et al. Macromolecular structure determination using X-rays, neutrons and electrons: recent developments in Phenix. *Acta Crystallogr. D Struct. Biol.* **75**, 861–877 (2019).
58. Moriarty, N. W., Grosse-Kunstleve, R. W. & Adams, P. D. electronic ligand builder and optimization workbench (eLBOW): a tool for ligand coordinate and restraint generation. *Acta Crystallogr. D Biol. Crystallogr.* **65**, 1074–1080 (2009).

**Acknowledgements** We are grateful to the staff of the Dubochet Center for Imaging (DCI-Lausanne) for cryo-imaging and preliminary data analysis. We thank Y. Polikanov from the University of Illinois at Chicago for providing the plasmid for the over-expression of the CCA-adding enzyme. We also thank C. Crucifix from the IGBMC cryo-EM platform for her expertise in grid preparation. This work was supported by La Fondation pour la Recherche Médicale grant no. DEQ20181039600 (to M.Y.).

**Author contributions** M.Y. and G.Y. conceived the project, N.M. conducted all biochemical experiments, and N.M and A.M. collected cryo-EM data. Main data analysis was performed by N.M. L.J. and A.M. also contributed to the data analysis. N.M. prepared the manuscript. G.Y. reviewed and edited the manuscript. G.Y. supervised the project. All authors gave their input in the preparation of the final manuscript.

**Competing interests** The authors declare no competing interests.

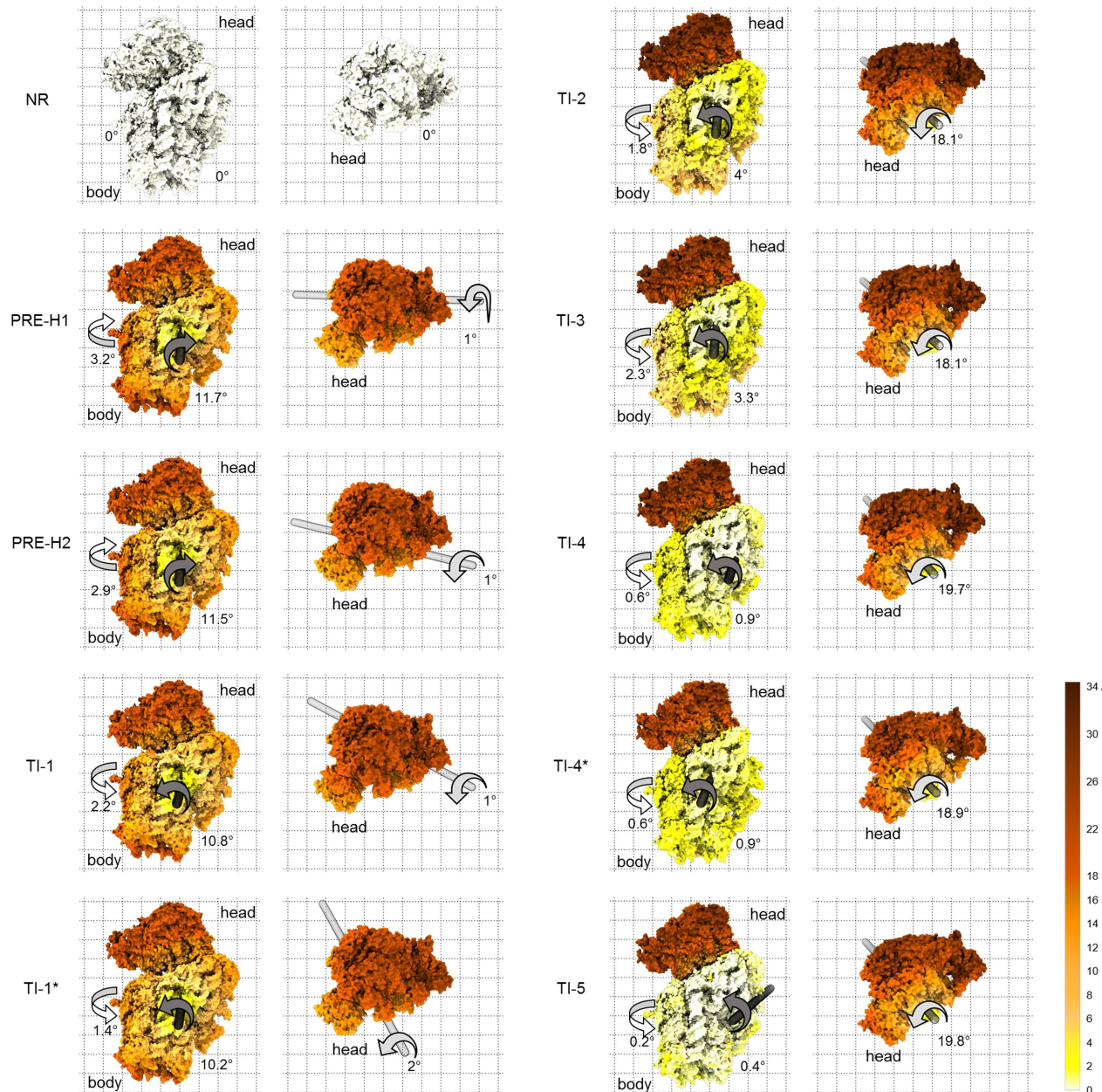
## Additional information

**Supplementary information** The online version contains supplementary material available at <https://doi.org/10.1038/s41586-023-06780-4>.

**Correspondence and requests for materials** should be addressed to Gulnara Yusupova.

**Peer review information** *Nature* thanks the anonymous reviewers for their contribution to the peer review of this work.

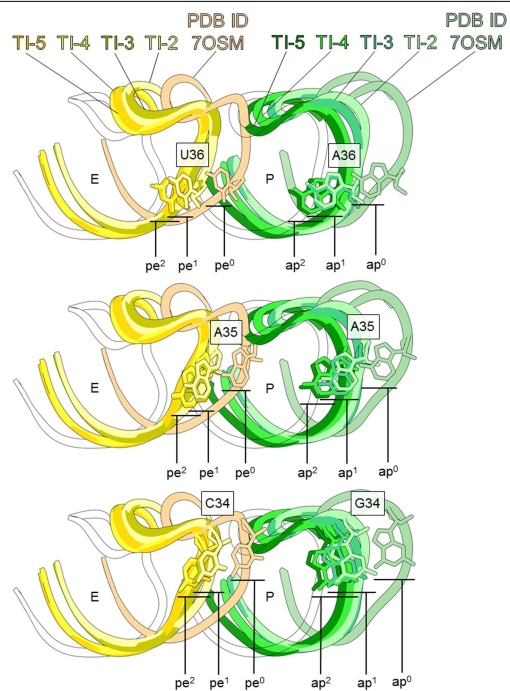
**Reprints and permissions information** is available at <http://www.nature.com/reprints>.



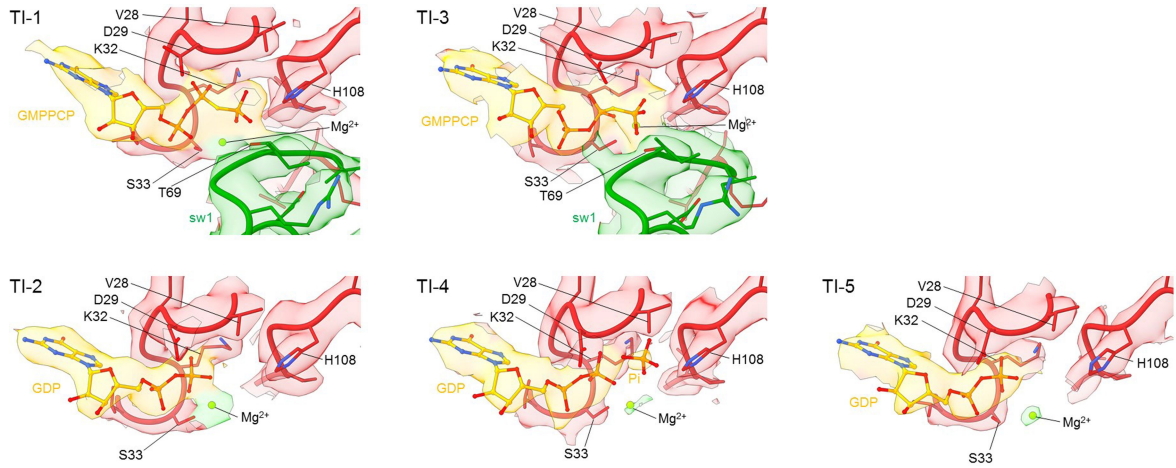
**Extended Data Fig. 1 | Large-scale conformational changes of the small ribosomal subunit.** Intersubunit view of the full SSU (left grid) and a zoomed top view of the SSU head domain (right grid) for each solved translocation complex. SSU is coloured on the basis of root-mean-square deviation values of atomic positions relative to the non-rotated (NR) state by 25S alignment. White

arrows indicate shoulder domain closure (upwards) or opening (downwards). Dark grey arrows indicate small subunit rotation (clockwise) or back-rotation (anti-clockwise) around the rotation axes shown in black. Light grey arrows indicate forward tilting or swiveling motions around the axes shown in light gray. All angles are calculated relative to the NR state.

# Article

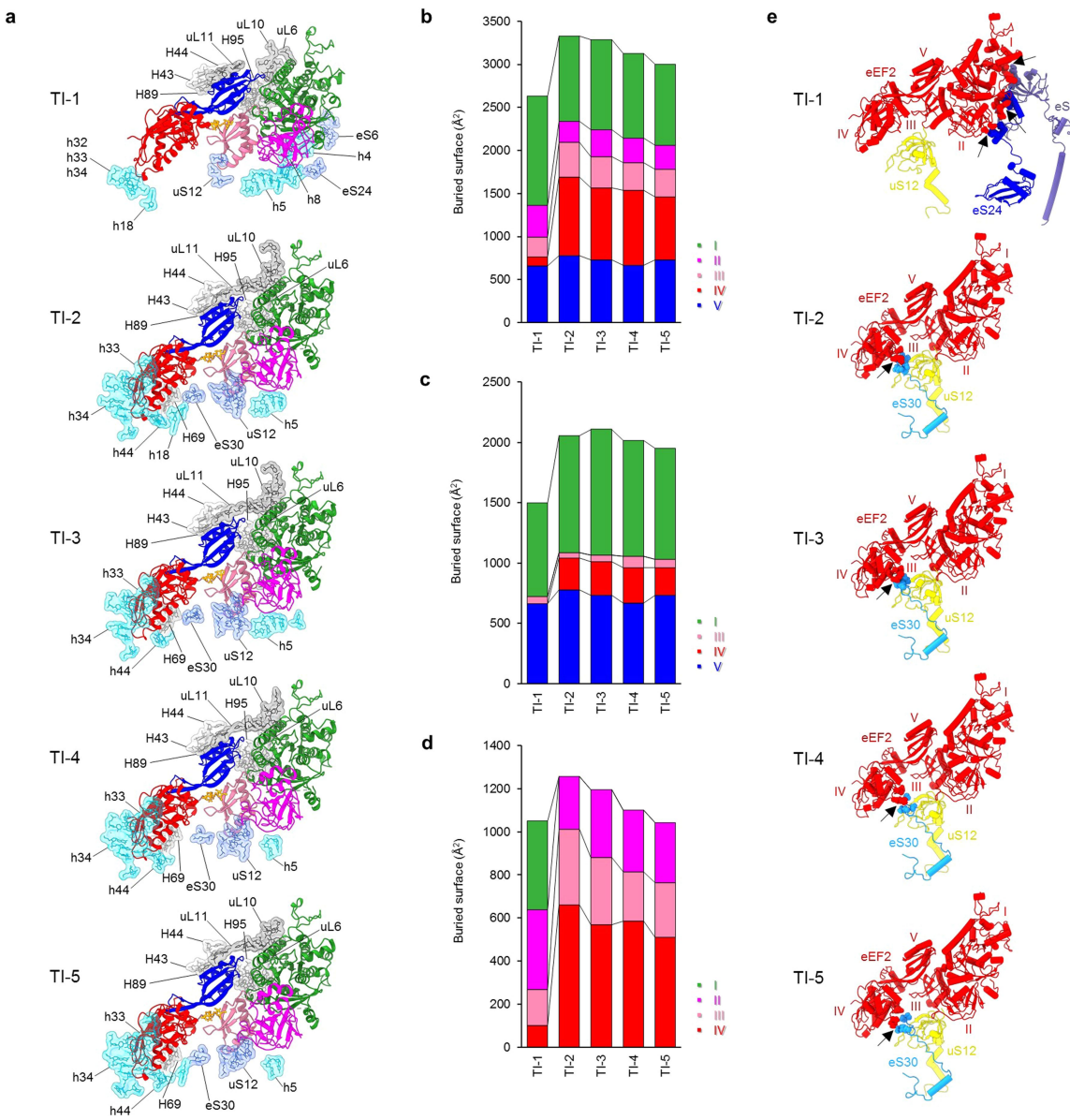


**Extended Data Fig. 2 | Progressive anticodon advancement in chimeric states of translocation.** Positions of peptidyl- (green) and deacyl-tRNA (yellow) anticodons in chimeric states of translocation TI-2 to TI-5 relative to final positions observed in the NR state (white) and the early chimeric ap<sup>0</sup>/P-pe<sup>0</sup>/E state (PDB ID 7OSM). Individually displayed anticodon nucleotides (top to bottom in the 3' – 5' direction) reveal distinct SSU sub-chimeric states: ap<sup>1</sup>-pe<sup>1</sup> (in TI-2 and TI-3) and ap<sup>2</sup>-pe<sup>2</sup> (in TI-4 and TI-5).



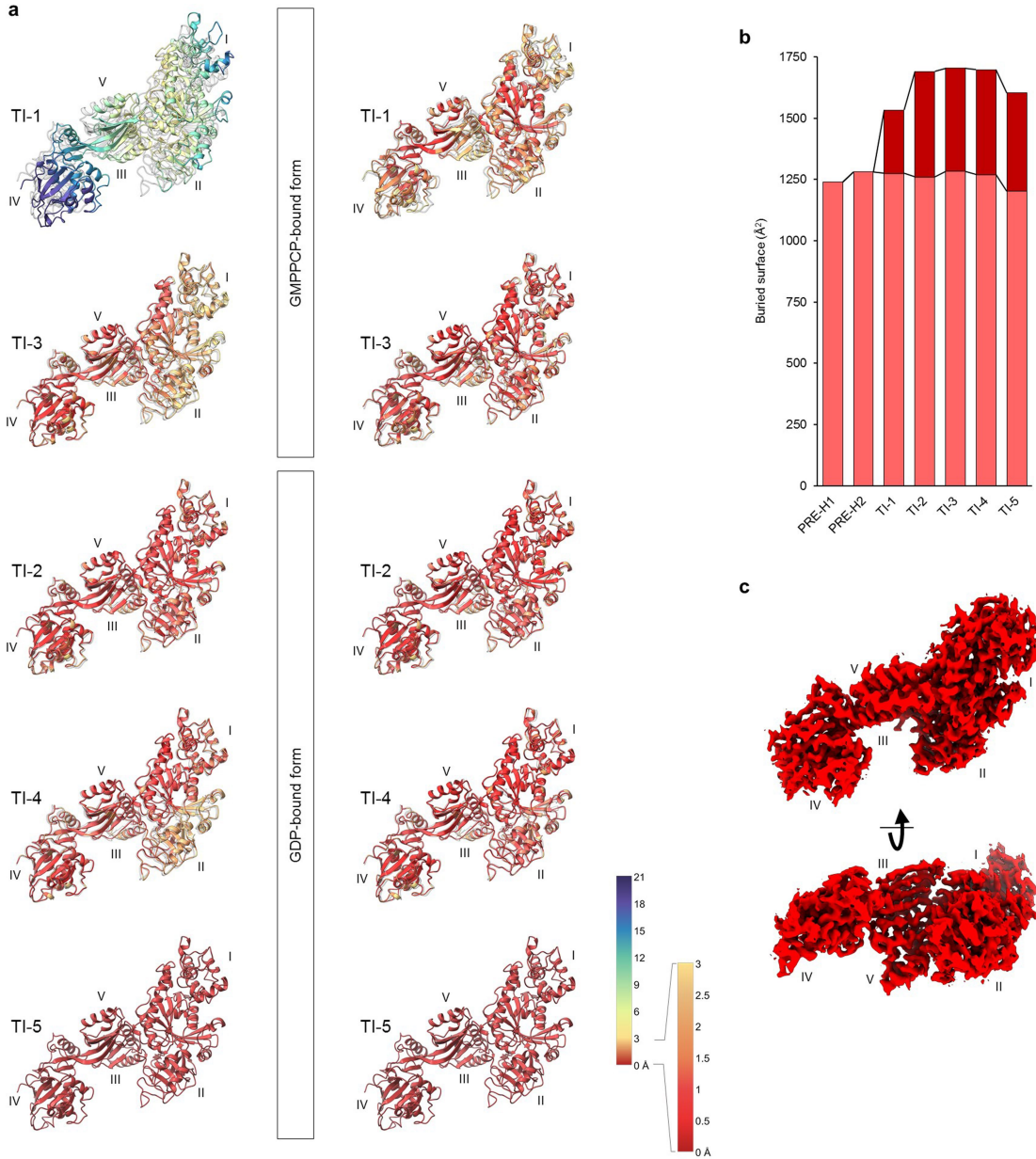
**Extended Data Fig. 3 | Nucleotide-binding pockets of eEF2 in translocation intermediates from TI-1 to TI-5.** Unfiltered, unsharpened maps ( $\sigma = 3$ ) of the nucleotide-binding pocket found in domain I of eEF2 (red). TI-1 and TI-3 show

density for the non-hydrolysable analogue of GTP (GMPPCP) and switch loop 1 (sw1). GDP-containing TI-2, TI-4 and TI-5 show no density for sw1. Additional density corresponding to inorganic phosphate was identified in TI-4.



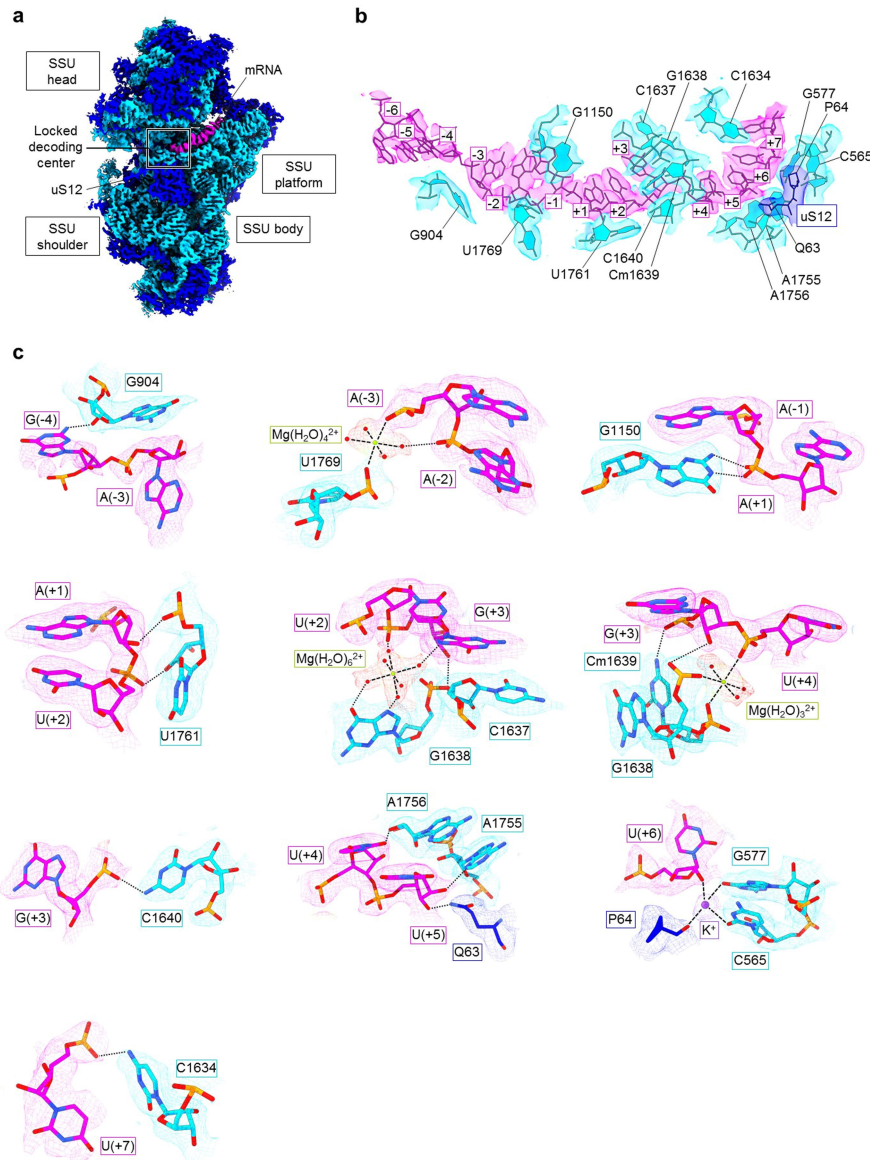
**Extended Data Fig. 4 | eEF2 interactions with the eukaryotic 80 S ribosome.** **a**, Contacts of eEF2 domains (I in green, II in magenta, III in pink, IV in red, and V in blue) with ribosomal elements of large 60 S (RNA in light grey and proteins in dark grey) and small 40 S subunit (RNA in light blue and proteins in dark blue) in translocation intermediate complexes TI-1 to TI-5. Sordarin is depicted in orange.

**b-d**, Quantification of contact areas of eEF2 domains I to V with 80 S, in **b**, large 60 S subunit, in **c**, and small 40 S subunit, in **d**. Eukaryote-specific interactions between eEF2 and SSU proteins eS6 and eS24 during factor recruitment in early translocation (TI-1), and eS30 once eEF2 is fully accommodated on 80 S (TI-2 to TI-5). Black arrows indicate areas of eukaryote-specific contacts.



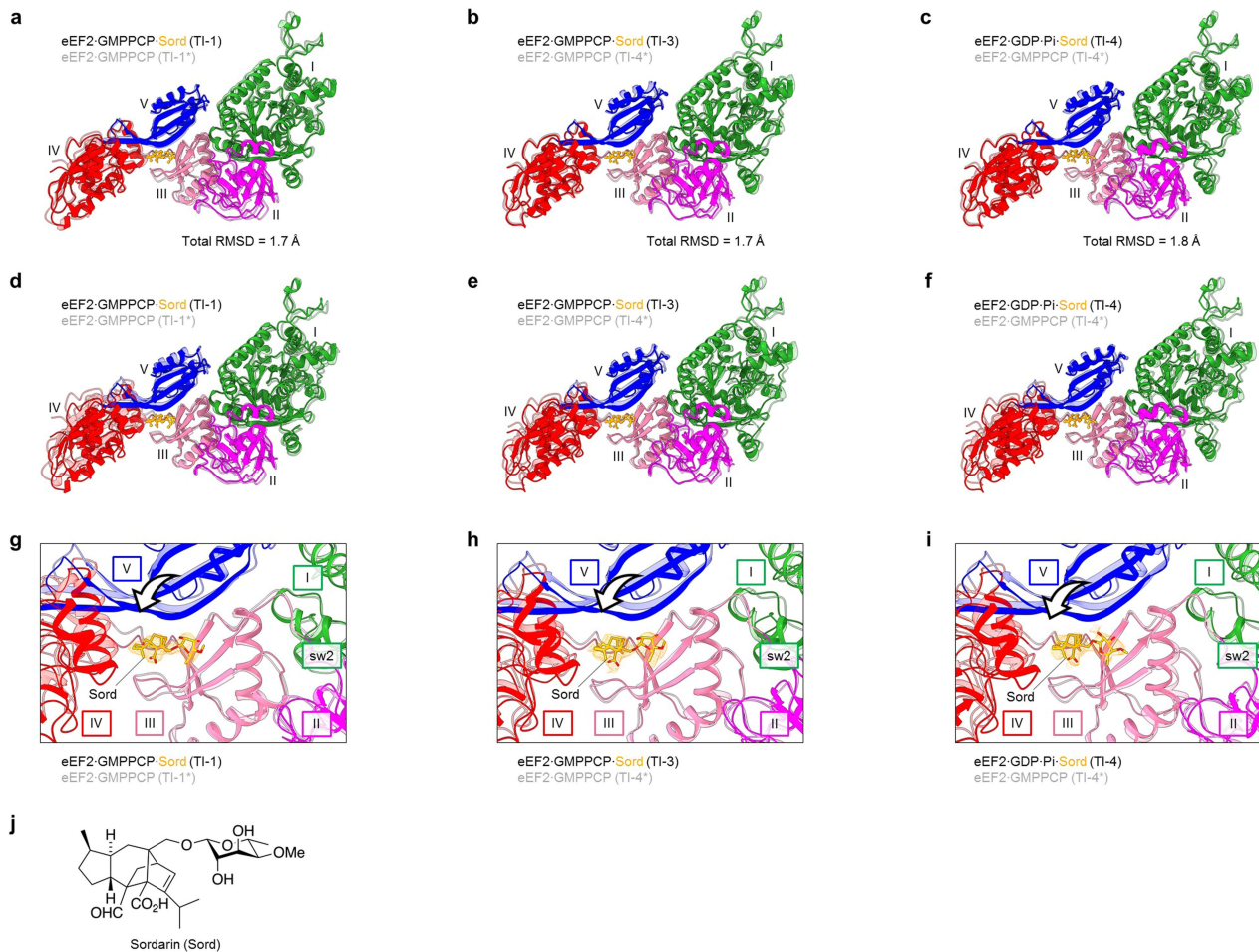
**Extended Data Fig. 5 | Conformational adaptations of eEF2 and contact areas with the tRNA<sub>2</sub>-mRNA translocating module.** **a**, Alignment on 25 S (left) and global eEF2 alignment (right) on eEF2 in TI-5 for GMPPCP bound intermediates TI-1 and TI-3, and GDP-containing intermediates TI-2, TI-4 and TI-5. Atoms are colored on the basis of root-mean-square deviation values of atomic positions

relative to TI-5. **b**, Buried surface measurements corresponding to contacts of the tRNA<sub>2</sub>-mRNA module with 80 S ribosome (pink) and domain IV of eEF2 (red) in the course of elongation from PRE-H1 to TI-5. **c**, Unfiltered, unsharpened density of *S. cerevisiae* eEF2 (e.g. TI-4) contoured at  $\sigma = 3$ .



**Extended Data Fig. 6 | mRNA path on the small subunit of the eukaryotic 80 S ribosome.** **a**, Lateral view of the full 40 S small subunit (SSU) of the eukaryotic 80 S ribosome trapped in the PRE-hybrid-1 reconstruction (PRE-H1) reveals the path of messenger RNA (magenta) at the SSU head-body domain interface. Unsharpened, unfiltered high-resolution cryo-EM maps are shown at  $\sigma = 3.5$ . 18 S ribosomal RNA and SSU proteins are colored in light and dark blue,

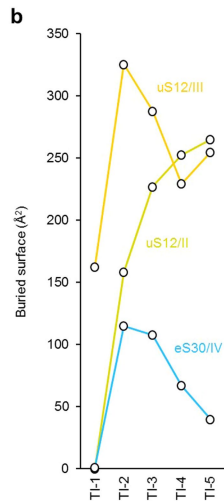
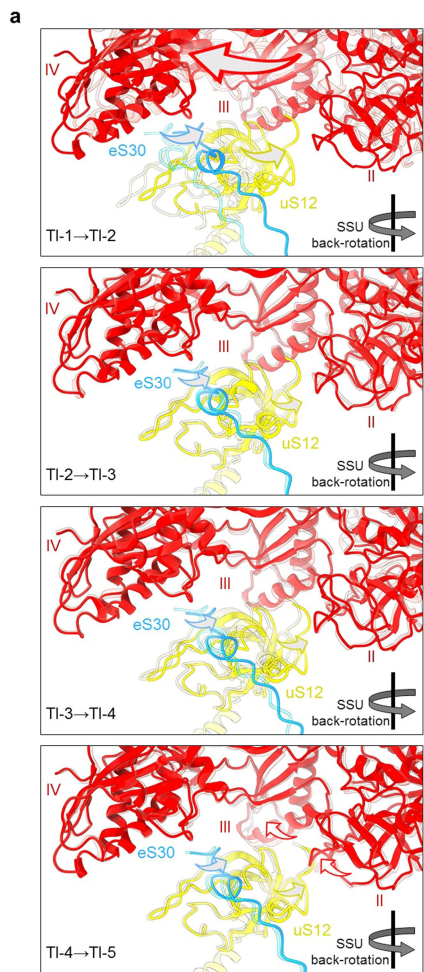
respectively. **b**, Zoom on the thirteen nucleotide-long messenger RNA and interacting residues of 18 S rRNA and the conserved SSU protein uS12. -1 indicates the first nucleotide of the start codon. **c**, Close-up view of the interactions between messenger RNA and ribosomal SSU elements in the PRE-H1 complex.  $\pi$ - $\pi$  stacking is found between -1 and G1150, while the p- $\pi$  effect is observed in the following interacting pairs: -3 and G904, and +3 and C1637.



**Extended Data Fig. 7 | Effect of sordarin binding to eEF2 in the context of eukaryotic translocation.** **a-c**, Global alignments reflecting general conservation of overall eEF2 conformation during early, in **a**, and late states of translocation, in **b** and **c**. **d-f**, Domain III alignment shows displacement of eEF2 domain V towards the interface with domain III. **g-l**, Zoom on the sordardin binding site for respective structural superimpositions on eEF2 domain III, as shown in **d-f**. The arrow indicates the displacement of domain V relative to

domain III. Remodelling of the switch loop 2 (sw2) has not been observed. Structural alignments are performed for late translocation states before, in **b**, **e** and **h**, and after GTP hydrolysis, in **c**, **f** and **i**. eEF2 domains are colored as follows: domain I in green, domain II in magenta, domain III in pink, domain IV in red, and domain V in blue. Unfiltered, unsharpened of sordarin is shown at  $\sigma = 4$  and depicted in orange. Lighter nuances correspond to structures without sordardin, TI-1\* and TI-4\*.j. Chemical structure of sordarin.

# Article



**Extended Data Fig. 8 | Interactions of eEF2 with small subunit proteins uS12 and eS30.** **a**, Inter-domain remodeling of eEF2 and conformational changes of SSU proteins uS12 and eS30 accompanying SSU back-rotation during respective transitions between translocation intermediates TI-1 to TI-5. **b**, Curves depicting contacts between SSU proteins uS12 with eEF2 domains II (dark yellow) and III (orange), and eS30 with domain IV (blue).

**Extended Data Table. 1 | Grid preparation, data collection and model validation parameters for NR, PRE-H1, TI-2, TI-4 and TI-5 complexes**

	Non-rotated	PRE-H1	TI-2	TI-4	TI-5
PDB	8CGN	8CCS	8CDR	8CEH	8CIV
EMDB	EMD-16648	EMD-16563	EMD-16594	EMD-16609	EMD-16684
<b>Grid</b>					
Manufacturer	Quantifoil	Quantifoil	Quantifoil	Quantifoil	Quantifoil
Type	Ultrathin Carbon				
Hole size/spacing	R 2/2				
Mesh	300 (Au)				
<b>Sample</b>					
Volume (µl)	3	3	3	3	3
Concentration (µM)	0.1	0.1	0.1	0.1	0.1
Blot time (s)	4	4	4	4	4
Temperature (°C)	9	9	9	9	9
Humidity (%)	95	95	95	95	95
<b>Data collection and processing</b>					
Microscope	Titan Krios G4				
Electron source	E-CFEG	E-CFEG	E-CFEG	E-CFEG	E-CFEG
Acceleration voltage (keV)	300	300	300	300	300
Camera	Falcon 4				
Nominal magnification	270,000	270,000	270,000	270,000	270,000
Pixel size	0.452	0.452	0.452	0.452	0.452
Total electron exposure (e-/Å²)	60	60	60	60	60
C2 aperture diameter (µm)	50	50	50	50	50
Nominal minimum defocus (nm)	400	400	400	400	400
Nominal maximum defocus (nm)	1,000	1,000	1,000	1,000	1,000
Number of collected micrographs	47,618	47,618	47,618	47,618	47,618
Number of used micrographs	45,282	45,282	45,282	45,282	45,282
Total number of extracted particles	616,978	616,978	616,978	616,978	616,978
Number of refined particles	442,508	442,508	442,508	442,508	442,508
Final number of complex particles	21,458	55,455	58,351	55,762	23,773
Resolution, unsharpened (Å)	2.28	1.97	2.04	2.05	2.47
FSC threshold	0.143	0.143	0.143	0.143	0.143
<b>Model-to-map</b>					
CC mask	0.81	0.85	0.84	0.85	0.84
CC volume	0.81	0.85	0.84	0.85	0.83
Resolution (Å)	2.64	2.23	2.40	2.41	2.82
FSC threshold	0.5	0.5	0.5	0.5	0.5
<b>Model</b>					
Atoms	201,528	201,697	207,753	207,126	207,374
Nucleotide residues	5,257	5,236	5,241	5,241	5,256
Protein residues	11,089	11,130	11,910	11,848	11,848
Bonds (RMSD)					
Length (Å)	0.003	0.005	0.007	0.008	0.009
Angles (°)	0.750	0.806	0.751	0.802	0.845
MolProbity score	2.09	2.14	2.14	2.20	2.10
Clash score	10.82	9.68	10.41	11.03	11.21
Ramachandran plot					
Outliers	0.02	0.08	0.02	0.05	0.05
Allowed	3.52	4.05	3.21	3.68	3.20
Favored	96.46	95.87	96.77	96.26	96.75
Ramachandran plot Z-score, whole	-0.73	-0.87	-0.87	-1.86	-0.85
Rotamer outliers (%)	2.55	2.81	3.34	3.25	2.76
Cβ outliers (%)	0.00	0.00	0.00	0.00	0.00
CaBLAM outliers (%)	4.19	4.14	4.06	4.40	4.16
ADP B factors, mean (Å²)					
Protein	62.17	57.88	64.08	69.57	60.91
Nucleotide	59.49	53.20	58.61	64.61	58.18

# Article

**Extended Data Table. 2 | Grid preparation, data collection and model validation parameters for TI-1, TI-3, PRE-H2, TI-1\* and TI-4\* complexes**

	TI-1	TI-3	PRE-H2	TI-1*	TI-4*
PDB	8CF5	8CG8	8CDL	8CKU	8CMJ
EMDB	EMD-16616	EMD-16634	EMD-16591	EMD-16702	EMD-16729
<b>Grid</b>					
Manufacturer	Quantifoil	Quantifoil	Quantifoil	Quantifoil	Quantifoil
Type	Ultrathin Carbon				
Hole size/spacing	R 2/2				
Mesh	300 (Au)				
<b>Sample</b>					
Volume (µl)	3	3	3	3	3
Concentration (µM)	0.1	0.1	0.1	0.1	0.1
Blot time (s)	4	4	4	4	4
Temperature (°C)	9	9	9	9	9
Humidity (%)	95	95	95	95	95
<b>Data collection</b>					
Microscope	Titan Krios G4				
Electron source	E-CFEG	E-CFEG	E-CFEG	E-CFEG	E-CFEG
Acceleration voltage (keV)	300	300	300	300	300
Camera	Falcon 4				
Nominal magnification	270,000	270,000	165,000	165,000	165,000
Pixel size	0.452	0.452	0.726	0.726	0.726
Total electron exposure (e-/Å²)	40	40	40	40	40
C2 aperture diameter (µm)	50	50	50	50	50
Nominal minimum defocus (nm)	400	400	400	400	400
Nominal maximum defocus (nm)	1,000	1,000	1,000	1,000	1,000
Number of collected micrographs	42,262	42,262	16,683	16,683	16,683
Number of used micrographs	39,533	39,533	16,654	16,654	16,654
Total number of extracted particles	514,460	514,460	624,552	624,552	624,552
Number of refined particles	393,786	393,789	561,498	561,498	561,498
Final number of complex particles	23,096	73,086	68,945	22,551	41,878
Resolution, unsharpened (Å)	2.71	2.57	2.72	3.11	3.79
FSC threshold	0.143	0.143	0.143	0.143	0.143
<b>Model-to-map</b>					
CC mask	0.83	0.80	0.85	0.79	0.73
CC volume	0.81	0.79	0.84	0.78	0.73
Resolution (Å)	2.96	2.96	2.99	3.62	4.63
FSC threshold	0.5	0.5	0.5	0.5	0.5
<b>Model</b>					
Atoms	208,161	207,325	201,553	207,340	202,630
Nucleotide residues	5,236	5,240	5,237	5,236	5,081
Protein residues	11,977	11,874	11,130	11,975	11,845
Bonds (RMSD)					
Length (Å)	0.008	0.07	0.04	0.06	0.004
Angles (°)	0.840	0.755	0.758	0.903	0.881
MolProbity score	1.90	1.83	1.80	1.95	2.07
Clash score	12.99	13.55	11.08	17.80	23.23
Ramachandran plot					
Outliers	0.09	0.02	0.06	0.03	0.04
Allowed	3.89	3.15	3.52	3.23	3.28
Favored	96.02	96.84	96.42	96.73	96.68
Ramachandran plot Z-score, whole	-0.91	-1.26	-0.70	-1.07	-1.54
Rotamer outliers (%)	0.25	0.05	0.17	0.05	0.04
Cβ outliers (%)	0.00	0.00	0.00	0.00	0.01
CaBLAM outliers (%)	3.99	4.22	4.12	4.17	4.31
ADP B factors, mean (Å²)					
Protein	54.45	62.40	80.47	86.61	126.50
Nucleotide	60.62	64.49	74.57	88.28	124.64

## Reporting Summary

Nature Portfolio wishes to improve the reproducibility of the work that we publish. This form provides structure for consistency and transparency in reporting. For further information on Nature Portfolio policies, see our [Editorial Policies](#) and the [Editorial Policy Checklist](#).

### Statistics

For all statistical analyses, confirm that the following items are present in the figure legend, table legend, main text, or Methods section.

n/a	Confirmed
<input checked="" type="checkbox"/>	<input type="checkbox"/> The exact sample size ( $n$ ) for each experimental group/condition, given as a discrete number and unit of measurement
<input checked="" type="checkbox"/>	<input type="checkbox"/> A statement on whether measurements were taken from distinct samples or whether the same sample was measured repeatedly
<input checked="" type="checkbox"/>	<input type="checkbox"/> The statistical test(s) used AND whether they are one- or two-sided <i>Only common tests should be described solely by name; describe more complex techniques in the Methods section.</i>
<input checked="" type="checkbox"/>	<input type="checkbox"/> A description of all covariates tested
<input checked="" type="checkbox"/>	<input type="checkbox"/> A description of any assumptions or corrections, such as tests of normality and adjustment for multiple comparisons
<input checked="" type="checkbox"/>	<input type="checkbox"/> A full description of the statistical parameters including central tendency (e.g. means) or other basic estimates (e.g. regression coefficient) AND variation (e.g. standard deviation) or associated estimates of uncertainty (e.g. confidence intervals)
<input checked="" type="checkbox"/>	<input type="checkbox"/> For null hypothesis testing, the test statistic (e.g. $F$ , $t$ , $r$ ) with confidence intervals, effect sizes, degrees of freedom and $P$ value noted <i>Give <math>P</math> values as exact values whenever suitable.</i>
<input checked="" type="checkbox"/>	<input type="checkbox"/> For Bayesian analysis, information on the choice of priors and Markov chain Monte Carlo settings
<input checked="" type="checkbox"/>	<input type="checkbox"/> For hierarchical and complex designs, identification of the appropriate level for tests and full reporting of outcomes
<input checked="" type="checkbox"/>	<input type="checkbox"/> Estimates of effect sizes (e.g. Cohen's $d$ , Pearson's $r$ ), indicating how they were calculated

*Our web collection on [statistics for biologists](#) contains articles on many of the points above.*

### Software and code

Policy information about [availability of computer code](#)

Data collection Single-particle datasets were acquired at the Dubochet Center for Imaging of EPFL and the University of Lausanne (DCI-Lausanne) on a 300 kV Titan Krios G4i transmission electron microscope (Thermo Fisher Scientific) equipped with a Cold FEG emission gun, SelectrisX energy filter and a Falcon IV direct electron detector. Datasets were collected using the EPU automated software (Thermo Fisher Scientific).

Data analysis Single-particle cryo-EM datasets were processed using Cryosparc v3.3. The model was built using Coot v0.8.9 and refined in Phenix v1.19.

For manuscripts utilizing custom algorithms or software that are central to the research but not yet described in published literature, software must be made available to editors and reviewers. We strongly encourage code deposition in a community repository (e.g. GitHub). See the Nature Portfolio [guidelines for submitting code & software](#) for further information.

### Data

Policy information about [availability of data](#)

All manuscripts must include a [data availability statement](#). This statement should provide the following information, where applicable:

- Accession codes, unique identifiers, or web links for publicly available datasets
- A description of any restrictions on data availability
- For clinical datasets or third party data, please ensure that the statement adheres to our [policy](#)

Atomic coordinates and cryo-EM maps generated during this study are available through the Protein Data Bank (PDB) and the Electron Microscopy Databank (EMDB). The complexes have been deposited under following accession codes: PRE-H1 (8CCS, EMD-16563), PRE-H2 (8CDL, EMD- 16591), TI-1 (8CF5, EMD-16616),

TI-2 (8CDR, EMD-16594), TI-3 (8CG8, EMD-16634), TI-4 (8CEH, EMD-16609), TI-5 (8CIV, EMD-16684), NR (8CGN, EMD-16648), TI-1\* (8CKU, EMD-16702), TI-4\* (8CMJ, EMD-16729).

## Research involving human participants, their data, or biological material

Policy information about studies with [human participants or human data](#). See also policy information about [sex, gender \(identity/presentation\), and sexual orientation](#) and [race, ethnicity and racism](#).

### Reporting on sex and gender

*Use the terms sex (biological attribute) and gender (shaped by social and cultural circumstances) carefully in order to avoid confusing both terms. Indicate if findings apply to only one sex or gender; describe whether sex and gender were considered in study design; whether sex and/or gender was determined based on self-reporting or assigned and methods used.*  
*Provide in the source data disaggregated sex and gender data, where this information has been collected, and if consent has been obtained for sharing of individual-level data; provide overall numbers in this Reporting Summary. Please state if this information has not been collected.*

*Report sex- and gender-based analyses where performed, justify reasons for lack of sex- and gender-based analysis.*

### Reporting on race, ethnicity, or other socially relevant groupings

*Please specify the socially constructed or socially relevant categorization variable(s) used in your manuscript and explain why they were used. Please note that such variables should not be used as proxies for other socially constructed/relevant variables (for example, race/ethnicity should not be used as a proxy for socioeconomic status).*  
*Provide clear definitions of the relevant terms used, how they were provided (by the participants/respondents, the researchers, or third parties), and the method(s) used to classify people into the different categories (e.g. self-report, census or administrative data, social media data, etc.)*

*Please provide details about how you controlled for confounding variables in your analyses.*

### Population characteristics

*Describe the covariate-relevant population characteristics of the human research participants (e.g. age, genotypic information, past and current diagnosis and treatment categories). If you filled out the behavioural & social sciences study design questions and have nothing to add here, write "See above."*

### Recruitment

*Describe how participants were recruited. Outline any potential self-selection bias or other biases that may be present and how these are likely to impact results.*

### Ethics oversight

*Identify the organization(s) that approved the study protocol.*

Note that full information on the approval of the study protocol must also be provided in the manuscript.

## Field-specific reporting

Please select the one below that is the best fit for your research. If you are not sure, read the appropriate sections before making your selection.

Life sciences

Behavioural & social sciences

Ecological, evolutionary & environmental sciences

For a reference copy of the document with all sections, see [nature.com/documents/nr-reporting-summary-flat.pdf](https://nature.com/documents/nr-reporting-summary-flat.pdf)

## Life sciences study design

All studies must disclose on these points even when the disclosure is negative.

### Sample size

The number of micrographs acquired for each data collection was determined by the number of particles required to achieve high-resolution of ribosomal reconstructions.

### Data exclusions

Cryo-EM processing is available in the Methods section.

### Replication

Cryo-EM data processing was performed according to standard methods applied to ribosomal complexes. Variability analyses performed on datasets collected on different microscopes resulted in equivalent class distributions.

### Randomization

No randomization was required for the reported experiments. All variables could be controlled.

### Blinding

Blinding was not applicable. The study did not require randomization and/or group allocation. All samples were of known composition and concentration.

## Behavioural & social sciences study design

All studies must disclose on these points even when the disclosure is negative.

### Study description

Briefly describe the study type including whether data are quantitative, qualitative, or mixed-methods (e.g. qualitative cross-sectional, quantitative experimental, mixed-methods case study).

### Research sample

State the research sample (e.g. Harvard university undergraduates, villagers in rural India) and provide relevant demographic

Research sample	<i>Information (e.g. age, sex) and indicate whether the sample is representative. Provide a rationale for the study sample chosen. For studies involving existing datasets, please describe the dataset and source.</i>
Sampling strategy	<i>Describe the sampling procedure (e.g. random, snowball, stratified, convenience). Describe the statistical methods that were used to predetermine sample size OR if no sample-size calculation was performed, describe how sample sizes were chosen and provide a rationale for why these sample sizes are sufficient. For qualitative data, please indicate whether data saturation was considered, and what criteria were used to decide that no further sampling was needed.</i>
Data collection	<i>Provide details about the data collection procedure, including the instruments or devices used to record the data (e.g. pen and paper, computer, eye tracker, video or audio equipment) whether anyone was present besides the participant(s) and the researcher, and whether the researcher was blind to experimental condition and/or the study hypothesis during data collection.</i>
Timing	<i>Indicate the start and stop dates of data collection. If there is a gap between collection periods, state the dates for each sample cohort.</i>
Data exclusions	<i>If no data were excluded from the analyses, state so OR if data were excluded, provide the exact number of exclusions and the rationale behind them, indicating whether exclusion criteria were pre-established.</i>
Non-participation	<i>State how many participants dropped out/declined participation and the reason(s) given OR provide response rate OR state that no participants dropped out/declined participation.</i>
Randomization	<i>If participants were not allocated into experimental groups, state so OR describe how participants were allocated to groups, and if allocation was not random, describe how covariates were controlled.</i>

## Ecological, evolutionary & environmental sciences study design

All studies must disclose on these points even when the disclosure is negative.

Study description	<i>Briefly describe the study. For quantitative data include treatment factors and interactions, design structure (e.g. factorial, nested, hierarchical), nature and number of experimental units and replicates.</i>
Research sample	<i>Describe the research sample (e.g. a group of tagged <i>Passer domesticus</i>, all <i>Stenocereus thurberi</i> within Organ Pipe Cactus National Monument), and provide a rationale for the sample choice. When relevant, describe the organism taxa, source, sex, age range and any manipulations. State what population the sample is meant to represent when applicable. For studies involving existing datasets, describe the data and its source.</i>
Sampling strategy	<i>Note the sampling procedure. Describe the statistical methods that were used to predetermine sample size OR if no sample-size calculation was performed, describe how sample sizes were chosen and provide a rationale for why these sample sizes are sufficient.</i>
Data collection	<i>Describe the data collection procedure, including who recorded the data and how.</i>
Timing and spatial scale	<i>Indicate the start and stop dates of data collection, noting the frequency and periodicity of sampling and providing a rationale for these choices. If there is a gap between collection periods, state the dates for each sample cohort. Specify the spatial scale from which the data are taken.</i>
Data exclusions	<i>If no data were excluded from the analyses, state so OR if data were excluded, describe the exclusions and the rationale behind them, indicating whether exclusion criteria were pre-established.</i>
Reproducibility	<i>Describe the measures taken to verify the reproducibility of experimental findings. For each experiment, note whether any attempts to repeat the experiment failed OR state that all attempts to repeat the experiment were successful.</i>
Randomization	<i>Describe how samples/organisms/participants were allocated into groups. If allocation was not random, describe how covariates were controlled. If this is not relevant to your study, explain why.</i>
Blinding	<i>Describe the extent of blinding used during data acquisition and analysis. If blinding was not possible, describe why OR explain why blinding was not relevant to your study.</i>

Did the study involve field work?  Yes  No

## Field work, collection and transport

Field conditions	<i>Describe the study conditions for field work, providing relevant parameters (e.g. temperature, rainfall).</i>
Location	<i>State the location of the sampling or experiment, providing relevant parameters (e.g. latitude and longitude, elevation, water depth).</i>
Access & import/export	<i>Describe the efforts you have made to access habitats and to collect and import/export your samples in a responsible manner and in compliance with local, national and international laws, noting any permits that were obtained (give the name of the issuing authority, the date of issue, and any identifying information).</i>

## Disturbance

Describe any disturbance caused by the study and how it was minimized.

# Reporting for specific materials, systems and methods

We require information from authors about some types of materials, experimental systems and methods used in many studies. Here, indicate whether each material, system or method listed is relevant to your study. If you are not sure if a list item applies to your research, read the appropriate section before selecting a response.

## Materials & experimental systems

n/a	Involved in the study
<input checked="" type="checkbox"/>	Antibodies
<input checked="" type="checkbox"/>	Eukaryotic cell lines
<input checked="" type="checkbox"/>	Palaeontology and archaeology
<input checked="" type="checkbox"/>	Animals and other organisms
<input checked="" type="checkbox"/>	Clinical data
<input checked="" type="checkbox"/>	Dual use research of concern
<input checked="" type="checkbox"/>	Plants

## Methods

n/a	Involved in the study
<input checked="" type="checkbox"/>	ChIP-seq
<input checked="" type="checkbox"/>	Flow cytometry
<input checked="" type="checkbox"/>	MRI-based neuroimaging

## Antibodies

### Antibodies used

Describe all antibodies used in the study; as applicable, provide supplier name, catalog number, clone name, and lot number.

### Validation

Describe the validation of each primary antibody for the species and application, noting any validation statements on the manufacturer's website, relevant citations, antibody profiles in online databases, or data provided in the manuscript.

## Eukaryotic cell lines

Policy information about [cell lines](#) and [Sex and Gender in Research](#)

### Cell line source(s)

State the source of each cell line used and the sex of all primary cell lines and cells derived from human participants or vertebrate models.

### Authentication

Describe the authentication procedures for each cell line used OR declare that none of the cell lines used were authenticated.

### Mycoplasma contamination

Confirm that all cell lines tested negative for mycoplasma contamination OR describe the results of the testing for mycoplasma contamination OR declare that the cell lines were not tested for mycoplasma contamination.

### Commonly misidentified lines (See [ICLAC](#) register)

Name any commonly misidentified cell lines used in the study and provide a rationale for their use.

## Palaeontology and Archaeology

### Specimen provenance

Provide provenance information for specimens and describe permits that were obtained for the work (including the name of the issuing authority, the date of issue, and any identifying information). Permits should encompass collection and, where applicable, export.

### Specimen deposition

Indicate where the specimens have been deposited to permit free access by other researchers.

### Dating methods

If new dates are provided, describe how they were obtained (e.g. collection, storage, sample pretreatment and measurement), where they were obtained (i.e. lab name), the calibration program and the protocol for quality assurance OR state that no new dates are provided.

Tick this box to confirm that the raw and calibrated dates are available in the paper or in Supplementary Information.

### Ethics oversight

Identify the organization(s) that approved or provided guidance on the study protocol, OR state that no ethical approval or guidance was required and explain why not.

Note that full information on the approval of the study protocol must also be provided in the manuscript.

## Animals and other research organisms

Policy information about [studies involving animals](#); [ARRIVE guidelines](#) recommended for reporting animal research, and [Sex and Gender in Research](#)

### Laboratory animals

*For laboratory animals, report species, strain and age OR state that the study did not involve laboratory animals.*

### Wild animals

*Provide details on animals observed in or captured in the field; report species and age where possible. Describe how animals were caught and transported and what happened to captive animals after the study (if killed, explain why and describe method; if released, say where and when) OR state that the study did not involve wild animals.*

### Reporting on sex

*Indicate if findings apply to only one sex; describe whether sex was considered in study design, methods used for assigning sex. Provide data disaggregated for sex where this information has been collected in the source data as appropriate; provide overall numbers in this Reporting Summary. Please state if this information has not been collected. Report sex-based analyses where performed, justify reasons for lack of sex-based analysis.*

### Field-collected samples

*For laboratory work with field-collected samples, describe all relevant parameters such as housing, maintenance, temperature, photoperiod and end-of-experiment protocol OR state that the study did not involve samples collected from the field.*

### Ethics oversight

*Identify the organization(s) that approved or provided guidance on the study protocol, OR state that no ethical approval or guidance was required and explain why not.*

Note that full information on the approval of the study protocol must also be provided in the manuscript.

## Clinical data

Policy information about [clinical studies](#)

All manuscripts should comply with the ICMJE [guidelines for publication of clinical research](#) and a completed [CONSORT checklist](#) must be included with all submissions.

### Clinical trial registration

*Provide the trial registration number from ClinicalTrials.gov or an equivalent agency.*

### Study protocol

*Note where the full trial protocol can be accessed OR if not available, explain why.*

### Data collection

*Describe the settings and locales of data collection, noting the time periods of recruitment and data collection.*

### Outcomes

*Describe how you pre-defined primary and secondary outcome measures and how you assessed these measures.*

## Dual use research of concern

Policy information about [dual use research of concern](#)

### Hazards

Could the accidental, deliberate or reckless misuse of agents or technologies generated in the work, or the application of information presented in the manuscript, pose a threat to:

No	Yes
<input type="checkbox"/>	<input type="checkbox"/> Public health
<input type="checkbox"/>	<input type="checkbox"/> National security
<input type="checkbox"/>	<input type="checkbox"/> Crops and/or livestock
<input type="checkbox"/>	<input type="checkbox"/> Ecosystems
<input type="checkbox"/>	<input type="checkbox"/> Any other significant area

## Experiments of concern

Does the work involve any of these experiments of concern:

- |                          |   |
|--------------------------|---|
| No                       | Yes   |
| <input type="checkbox"/> | Demonstrate how to render a vaccine ineffective                             |
| <input type="checkbox"/> | Confer resistance to therapeutically useful antibiotics or antiviral agents |
| <input type="checkbox"/> | Enhance the virulence of a pathogen or render a nonpathogen virulent        |
| <input type="checkbox"/> | Increase transmissibility of a pathogen                                     |
| <input type="checkbox"/> | Alter the host range of a pathogen  |
| <input type="checkbox"/> | Enable evasion of diagnostic/detection modalities                           |
| <input type="checkbox"/> | Enable the weaponization of a biological agent or toxin                     |
| <input type="checkbox"/> | Any other potentially harmful combination of experiments and agents         |

## Plants

### Seed stocks

Report on the source of all seed stocks or other plant material used. If applicable, state the seed stock centre and catalogue number. If plant specimens were collected from the field, describe the collection location, date and sampling procedures.

### Novel plant genotypes

Describe the methods by which all novel plant genotypes were produced. This includes those generated by transgenic approaches, gene editing, chemical/radiation-based mutagenesis and hybridization. For transgenic lines, describe the transformation method, the number of independent lines analyzed and the generation upon which experiments were performed. For gene-edited lines, describe the editor used, the endogenous sequence targeted for editing, the targeting guide RNA sequence (if applicable) and how the editor was applied.

### Authentication

Describe any authentication procedures for each seed stock used or novel genotype generated. Describe any experiments used to assess the effect of a mutation and, where applicable, how potential secondary effects (e.g. second site T-DNA insertions, mosaicism, off-target gene editing) were examined.

## ChIP-seq

### Data deposition

- Confirm that both raw and final processed data have been deposited in a public database such as [GEO](#).
- Confirm that you have deposited or provided access to graph files (e.g. BED files) for the called peaks.

### Data access links

*May remain private before publication.*

For "Initial submission" or "Revised version" documents, provide reviewer access links. For your "Final submission" document, provide a link to the deposited data.

### Files in database submission

Provide a list of all files available in the database submission.

### Genome browser session (e.g. [UCSC](#))

Provide a link to an anonymized genome browser session for "Initial submission" and "Revised version" documents only, to enable peer review. Write "no longer applicable" for "Final submission" documents.

## Methodology

### Replicates

Describe the experimental replicates, specifying number, type and replicate agreement.

### Sequencing depth

Describe the sequencing depth for each experiment, providing the total number of reads, uniquely mapped reads, length of reads and whether they were paired- or single-end.

### Antibodies

Describe the antibodies used for the ChIP-seq experiments; as applicable, provide supplier name, catalog number, clone name, and lot number.

### Peak calling parameters

Specify the command line program and parameters used for read mapping and peak calling, including the ChIP, control and index files used.

### Data quality

Describe the methods used to ensure data quality in full detail, including how many peaks are at FDR 5% and above 5-fold enrichment.

### Software

Describe the software used to collect and analyze the ChIP-seq data. For custom code that has been deposited into a community repository, provide accession details.

# Flow Cytometry

## Plots

Confirm that:

- The axis labels state the marker and fluorochrome used (e.g. CD4-FITC).
- The axis scales are clearly visible. Include numbers along axes only for bottom left plot of group (a 'group' is an analysis of identical markers).
- All plots are contour plots with outliers or pseudocolor plots.
- A numerical value for number of cells or percentage (with statistics) is provided.

## Methodology

### Sample preparation

*Describe the sample preparation, detailing the biological source of the cells and any tissue processing steps used.*

### Instrument

*Identify the instrument used for data collection, specifying make and model number.*

### Software

*Describe the software used to collect and analyze the flow cytometry data. For custom code that has been deposited into a community repository, provide accession details.*

### Cell population abundance

*Describe the abundance of the relevant cell populations within post-sort fractions, providing details on the purity of the samples and how it was determined.*

### Gating strategy

*Describe the gating strategy used for all relevant experiments, specifying the preliminary FSC/SSC gates of the starting cell population, indicating where boundaries between "positive" and "negative" staining cell populations are defined.*

- Tick this box to confirm that a figure exemplifying the gating strategy is provided in the Supplementary Information.

# Magnetic resonance imaging

## Experimental design

### Design type

*Indicate task or resting state; event-related or block design.*

### Design specifications

*Specify the number of blocks, trials or experimental units per session and/or subject, and specify the length of each trial or block (if trials are blocked) and interval between trials.*

### Behavioral performance measures

*State number and/or type of variables recorded (e.g. correct button press, response time) and what statistics were used to establish that the subjects were performing the task as expected (e.g. mean, range, and/or standard deviation across subjects).*

## Acquisition

### Imaging type(s)

*Specify: functional, structural, diffusion, perfusion.*

### Field strength

*Specify in Tesla*

### Sequence & imaging parameters

*Specify the pulse sequence type (gradient echo, spin echo, etc.), imaging type (EPI, spiral, etc.), field of view, matrix size, slice thickness, orientation and TE/TR/flip angle.*

### Area of acquisition

*State whether a whole brain scan was used OR define the area of acquisition, describing how the region was determined.*

### Diffusion MRI

- Used
- Not used

## Preprocessing

### Preprocessing software

*Provide detail on software version and revision number and on specific parameters (model/functions, brain extraction, segmentation, smoothing kernel size, etc.).*

### Normalization

*If data were normalized/standardized, describe the approach(es): specify linear or non-linear and define image types used for transformation OR indicate that data were not normalized and explain rationale for lack of normalization.*

### Normalization template

*Describe the template used for normalization/transformation, specifying subject space or group standardized space (e.g. original Talairach, MNI305, ICBM152) OR indicate that the data were not normalized.*

### Noise and artifact removal

*Describe your procedure(s) for artifact and structured noise removal, specifying motion parameters, tissue signals and physiological signals (heart rate, respiration).*

## Volume censoring

*Define your software and/or method and criteria for volume censoring, and state the extent of such censoring.*

## Statistical modeling &amp; inference

## Model type and settings

*Specify type (mass univariate, multivariate, RSA, predictive, etc.) and describe essential details of the model at the first and second levels (e.g. fixed, random or mixed effects; drift or auto-correlation).*

## Effect(s) tested

*Define precise effect in terms of the task or stimulus conditions instead of psychological concepts and indicate whether ANOVA or factorial designs were used.*

Specify type of analysis:  Whole brain  ROI-based  Both

## Statistic type for inference

*Specify voxel-wise or cluster-wise and report all relevant parameters for cluster-wise methods.*

(See [Eklund et al. 2016](#))

## Correction

*Describe the type of correction and how it is obtained for multiple comparisons (e.g. FWE, FDR, permutation or Monte Carlo).*

## Models &amp; analysis

n/a Involved in the study

- Functional and/or effective connectivity
- Graph analysis
- Multivariate modeling or predictive analysis

## Functional and/or effective connectivity

*Report the measures of dependence used and the model details (e.g. Pearson correlation, partial correlation, mutual information).*

## Graph analysis

*Report the dependent variable and connectivity measure, specifying weighted graph or binarized graph, subject- or group-level, and the global and/or node summaries used (e.g. clustering coefficient, efficiency, etc.).*

## Multivariate modeling and predictive analysis

*Specify independent variables, features extraction and dimension reduction, model, training and evaluation metrics.*